GTSE1 tunes microtubule stability for chromosome alignment and segregation by inhibiting the microtubule depolymerase MCAK

Shweta Bendre,[1] Arnaud Rondelet,[1] Conrad Hall,[2] Nadine Schmidt,[1] Yu-Chih Lin,[1] Gary J. Brouhard,[2] and Alexander W. Bird[1]

[1]Max Planck Institute of Molecular Physiology, 44227 Dortmund, Germany
[2]Department of Biology, McGill University, Montreal H3A 1B1, Quebec, Canada

The dynamic regulation of microtubules (MTs) during mitosis is critical for accurate chromosome segregation and genome stability. Cancer cell lines with hyperstabilized kinetochore MTs have increased segregation errors and elevated chromosomal instability (CIN), but the genetic defects responsible remain largely unknown. The MT depolymerase MCAK (mitotic centromere-associated kinesin) can influence CIN through its impact on MT stability, but how its potent activity is controlled in cells remains unclear. In this study, we show that GTSE1, a protein found overexpressed in aneuploid cancer cell lines and tumors, regulates MT stability during mitosis by inhibiting MCAK MT depolymerase activity. Cells lacking GTSE1 have defects in chromosome alignment and spindle positioning as a result of MT instability caused by excess MCAK activity. Reducing GTSE1 levels in CIN cancer cell lines reduces chromosome missegregation defects, whereas artificially inducing GTSE1 levels in chromosomally stable cells elevates chromosome missegregation and CIN. Thus, GTSE1 inhibition of MCAK activity regulates the balance of MT stability that determines the fidelity of chromosome alignment, segregation, and chromosomal stability.

Introduction

The precise regulation of microtubule (MT) dynamics is essential to the accurate execution of mitosis and the faithful segregation of chromosomes. Defects in the regulation of MT stability and dynamics can result in errors in spindle positioning and chromosome segregation, two processes found to be defective in cancers (Gordon et al., 2012; Noatynska et al., 2012). Persistent errors in chromosome segregation lead to chromosomal instability (CIN), the increased rate of gain or loss of chromosomes within a cell population. CIN is present in most solid tumors, and recent evidence suggests CIN plays a causal role in tumorigenesis (Schvartzman et al., 2010). The genetic and molecular defects that lead to CIN in tumors, however, remain largely unknown.

In several cancer cell lines with CIN, kinetochore–MT attachments are hyperstabilized (Bakhoum et al., 2009a). This hyperstabilization leads to an increased frequency of chromosome missegregation, and ultimately to CIN, as a result of a reduced ability of cells to correct erroneous kinetochore–MT attachments, in particular merotelic attachments, where one kinetochore is connected to MTs from both spindle poles (Bakhoum et al., 2009a,b). Cells must therefore be able to precisely regulate MT dynamics so that kinetochore MTs are dynamic enough to correct erroneous attachments, yet stable enough to efficiently capture and align chromosomes (Bakhoum et al., 2009a,b). The regulatory mechanisms by which cells are able to maintain this balance and avoid CIN remain unclear.

A major direct regulator of MT stability is the kinesin-13 MT depolymerase Kif2C/MCAK (mitotic centromere-associated kinesin). In vitro, MCAK has extremely potent depolymerase activity (Desai et al., 1999; Hunter et al., 2003; Helenius et al., 2006). In cells, reduction of MCAK activity leads to an increase in MT polymer (Rizk et al., 2009; Rankin and Wordeman, 2010). Kinetochore–MT attachments are also hyperstabilized, leading to defects in correcting merotelic attachments and in chromosome segregation (Maney et al., 1998; Kline-Smith et al., 2003; Bakhoum et al., 2009a). Excessive MCAK activity induced by the overexpression of MCAK leads to a loss of MT stability throughout the cell and to defects in the capture and alignment of chromosomes (Maney et al., 1998; Moore and Wordeman, 2004; Zhang et al., 2011). MCAK MT depolymerase activity must therefore be precisely controlled in time and cellular space to

Correspondence to Alexander W. Bird: alex.bird@mpi-dortmund.mpg.de

Abbreviations used: BAC, bacterial artificial chromosome; CIN, chromosomal instability; CRISPR, clustered regularly interspaced short palindromic repeats; FDAPA, fluorescence dissipation after photoactivation; MCAK, mitotic centromere-associated kinesin; MT, microtubule; PA, photoactivatable; TIRF, total internal reflection fluorescence.

The Rockefeller University Press $30.00
J. Cell Biol. Vol. 215 No. 5 631–647
https://doi.org/10.1083/jcb.201606081

ensure both chromosome alignment and segregation and to avoid CIN. Although interest in MCAK regulation has led to the identification of proteins that enhance or counteract MCAK activity in cells (Ohi et al., 2003; Jiang et al., 2009; Cross and Powers, 2011; Meunier and Vernos, 2011), only NuSAP (nucleolar spindle-associated protein) has been recently reported to attenuate MCAK activity via direct interaction (Li et al., 2016). In vitro studies of MCAK have uncovered potential mechanisms by which intramolecular rearrangements of MCAK can determine MT depolymerase activity (Ems-McClung et al., 2013; Burns et al., 2014; Talapatra et al., 2015). Based on this knowledge, proposed mechanisms for the direct regulation of MCAK activity in cells have thus largely relied on intramolecular rearrangements induced from interaction with MTs, nucleotide exchange, and phosphorylation by mitotic kinases (Cooper et al., 2009; Ems-McClung et al., 2013; Burns et al., 2014; Talapatra et al., 2015).

Because MCAK activity affects kinetochore–MT stability, its deregulation may impact CIN. Indeed, artificially destabilizing kinetochore MTs in CIN lines by overexpressing MCAK reduces chromosome missegregation and CIN (Bakhoum et al., 2009b). Although these key experiments point to the hyperstability of kinetochore MTs in cancer cell lines as a direct cause of CIN, they do not resolve the molecular genetic origin of this defect, as MCAK protein levels are not generally down-regulated in cancer cell lines or tumors (Bakhoum et al., 2009a; Sanhaji et al., 2011). Therefore, investigation into the cellular regulation of MCAK activity, as well as the molecular basis of kinetochore–MT hyperstabilization in cancer cells, is highly desirable.

GTSE1 is an MT-associated and EB1-dependent plus end tracking protein (Monte et al., 2000; Scolz et al., 2012). In interphase, recruitment of GTSE1 to growing MT plus ends by EB1 is required for cell migration. During mitosis, GTSE1 is heavily phosphorylated and no longer tracks MT plus ends nor interacts directly with the MT lattice but localizes to the mitotic spindle in a TACC3-dependent manner (Hubner et al., 2010; Scolz et al., 2012). GTSE1 expression levels are up-regulated in several tumor types and cancer cell lines and correlate with tumor grade and poor clinical outcome in breast cancers (Scolz et al., 2012), although it remains unknown whether GTSE1 overexpression facilitates tumorigenesis.

Here, we show that GTSE1 stabilizes MTs during mitosis to facilitate chromosome alignment by suppressing MCAK MT depolymerase activity. GTSE1 interacts with MCAK and inhibits its activity in vitro, thus extending our understanding of the mechanisms controlling MCAK activity. Perturbing the balance of the GTSE1–MCAK relationship in cancer cell lines influences CIN through its effect on MT stabilization: increasing GTSE1 expression in diploid cell lines leads to chromosome segregation defects and induces CIN, whereas depletion or knockout of the high GTSE1 levels in CIN cell lines reduces chromosome segregation defects in an MCAK-dependent manner. Thus, GTSE1 tunes MT stability in mitosis to ensure both chromosome alignment and accurate segregation by suppressing MCAK MT depolymerase activity.

Results

GTSE1 stabilizes MTs in mitosis and promotes correct spindle orientation

To investigate the role of GTSE1 during mitosis, we first reduced GTSE1 protein levels by RNAi in human U2OS cells and analyzed them by immunofluorescence (Figs. 1 A and S1 A). GTSE1-depleted mitotic cells displayed a loss of MT stability as observed by immunofluorescence labeling of tubulin. In >50% of cells depleted of GTSE1, astral MTs appeared absent or dramatically shortened in both prometaphase and metaphase cells (Fig. 1, A and B), and MT density within the inner spindle was significantly reduced (Fig. 1 C). We quantified the defect in astral MT stability via three additional analyses. First, we measured the length in three dimensions of the 10 longest astral MTs visible per cell from tubulin immunofluorescence. The length of the few visible astral MTs remaining after GTSE1 RNAi was less than half that of control cells (Fig. 1 D). Second, we calculated the mean length of all astral MTs per cell by calculating the mean distance between growing astral MT plus ends and the centrosome via EB1 protein immunofluorescence and again found a significant reduction (Fig. 1 E). Finally, we calculated the total number of growing astral MTs from EB1 staining and found a nearly 50% reduction after GTSE1 RNAi (Fig. 1 F).

To verify that the loss of MT stability after RNAi was specific to the depletion of GTSE1, we depleted GTSE1 in two independent and clonal cell lines containing stably integrated RNAi-resistant, GFP-tagged GTSE1 genes harbored on bacterial artificial chromosomes (BACs; $GTSE1^{WT(204)}$ and $GTSE1^{WT(212)}$; Bird et al., 2011; Scolz et al., 2012). After depletion of endogenous GTSE1, GTSE1-GFP localized to the mitotic spindle, which we also observed upon tagging of endogenous GTSE1 with GFP via CRISPR-Cas9 (clustered regularly interspaced short palindromic repeats)-mediated homologous recombination (Figs. 1 G and S2 A; Cong et al., 2013; Ran et al., 2013). RNAi-resistant GTSE1-GFP–expressing cells maintained astral MTs after GTSE1 RNAi, confirming specificity (Figs. 1 B and S1 B).

To further confirm the role for GTSE1 in MT stability, we knocked out the genomic copies of the GTSE1 gene in U2OS cells via CRISPR-Cas9 nuclease targeting (Cong et al., 2013; Ran et al., 2013). Interestingly, we were able to isolate viable clonal GTSE1 knockout cell lines, and two independently constructed knockout clones were subsequently analyzed ($GTSE1^{KO(1)}$ and $GTSE1^{KO(2)}$; Fig. S2, B–D). Both GTSE1 knockout cell lines displayed a significant destabilization of astral MTs in mitosis (Fig. 1, A, B, and D–F). Although spindle MT stability was compromised, neither knockout nor RNAi depletion of GTSE1 led to a change in spindle length (Fig. S2 E).

We previously found that the interaction between GTSE1 and EB1 is required for GTSE1's function in cell migration and MT-dependent focal adhesion disassembly (Scolz et al., 2012). To determine whether this interaction was important for the role of GTSE1 in mitotic MT stability, we analyzed cells expressing RNAi-resistant, BAC-based GTSE1 that does not interact with EB1 because of the mutation of conserved EB-binding (SxIP) motifs (Scolz et al., 2012). After depletion of endogenous GTSE1, SxIP-mutated GTSE1 was able to maintain astral stability similar to the wild-type GTSE1 gene (Figs. 1 B and S1 B). Thus, the interaction between GTSE1 and EB1 is not important for MT stability in prometaphase and metaphase.

GTSE1-depleted cells lacking astral MTs often displayed a defect in the positioning of the spindle within the cell, consistent with known roles of astral MT–cortex interactions in establishing spindle orientation (Pearson and Bloom, 2004). We quantified this defect in spindle orientation by measuring the angle of the spindle relative to the coverslip surface and found that cells depleted of GTSE1 more frequently failed to align the

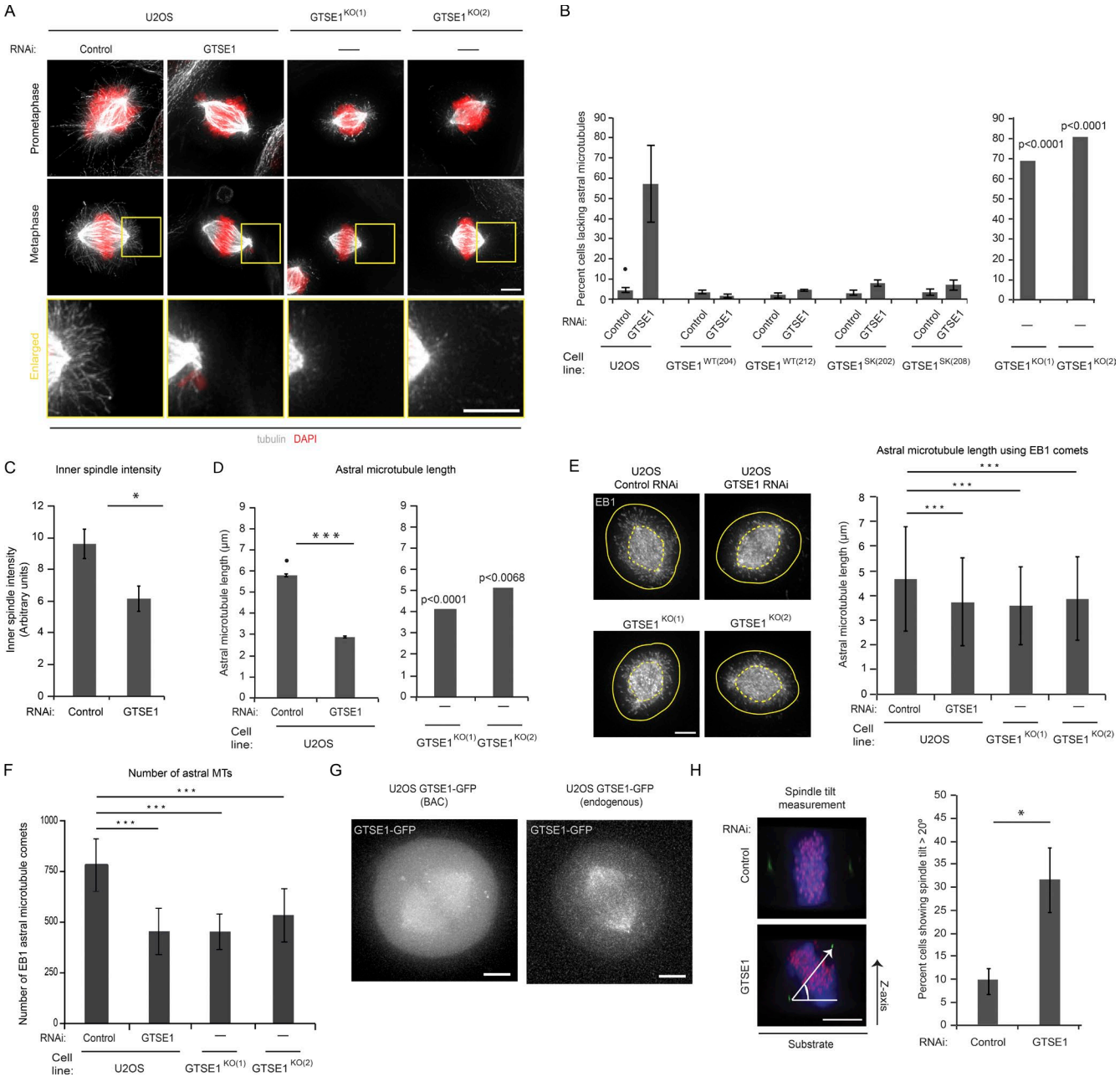

Figure 1. **GTSE1 stabilizes MTs in mitosis and promotes correct spindle orientation.** (A) Immunofluorescence images of U2OS cells after control RNAi, GTSE1 RNAi, and stable knockout of GTSE1 stained for DNA (DAPI) and MTs (tubulin) showing fewer astral MTs after reduced GTSE1 levels. (B) Quantification of the percentage of cells lacking astral MTs from immunofluorescence analysis as shown in A. The left graph shows control and GTSE1 RNAi in U2OS cells, two stable U2OS cell clones expressing RNAi-resistant GTSE1 ($GTSE1^{WT(204)}$ and $GTSE1^{WT(212)}$), and two stable U2OS cell clones expressing RNAi-resistant GTSE1 mutated to abolish interaction with EB1 ($GTSE1^{Sk(202)}$ and $GTSE1^{Sk(208)}$). $n > 150$ cells; 3 experiments per condition. The right graph shows two independent U2OS GTSE1 knockout clones. P-values were obtained from a χ^2 test comparing against the U2OS control condition (marked with •). $n > 100$ cells. (C) Quantification of inner-spindle tubulin fluorescence intensity from fixed U2OS cells stained for α-tubulin after control or GTSE1 RNAi. $n \geq 19$ per experiment per condition; 3 experiments. (D) Quantification of the mean length of astral MTs in three dimensions from immunofluorescence analysis as shown in A. 10 astral MTs were measured per cell. $n = 10$ cells per experiment per condition; 3 experiments. (E) Immunofluorescence images of U2OS cells after control RNAi, GTSE1 RNAi, and stable knockout of GTSE1 stained for EB1 showing fewer EB1 astral MT comets after GTSE1 RNAi. Graph shows quantification of astral MT length using the position of EB1 comets with respect to the centrosome. $n > 5{,}800$ astrals from 15 cells per condition; 1 experiment. P-values were obtained using a Kruskal-Wallis test followed by Conover-Iman test. (F) Quantification of the mean number of astral MTs per cell obtained by quantifying the number of EB1 comets in U2OS cells after control or GTSE1 RNAi and in $GTSE1^{KO(1)}$ and $GTSE1^{KO(2)}$ cells. $n \geq 13$ cells per condition; 1 experiment. (E and F) Error bars represent standard deviation. P-values were obtained using an analysis of variance and a Tukey's test. (G) Live-cell fluorescence images of metaphase U2OS cells expressing either BAC-expressed GTSE1-GFP ($GTSE1^{WT(212)}$) or endogenously tagged GTSE1-GFP. Both constructs localize to the spindle. (H) Analysis of spindle orientation. Images of mitotic cells viewed from the side and stained for DNA (blue), kinetochores (red), and centrioles (green) depict a cell with normal spindle alignment parallel to the substrate (top) and a cell with defective orientation (bottom). The angle of spindle tilt was calculated by determining the angle between the substrate and a line connecting both centrosomes, as depicted. Quantification of the percentage of metaphase cells with a spindle tilt angle >20° is shown. $n > 140$ cells; 3 experiments per condition. Bars, 5 µm. All error bars represent SEM unless otherwise specified. *, $P \leq 0.05$; ***, $P \leq 0.001$.

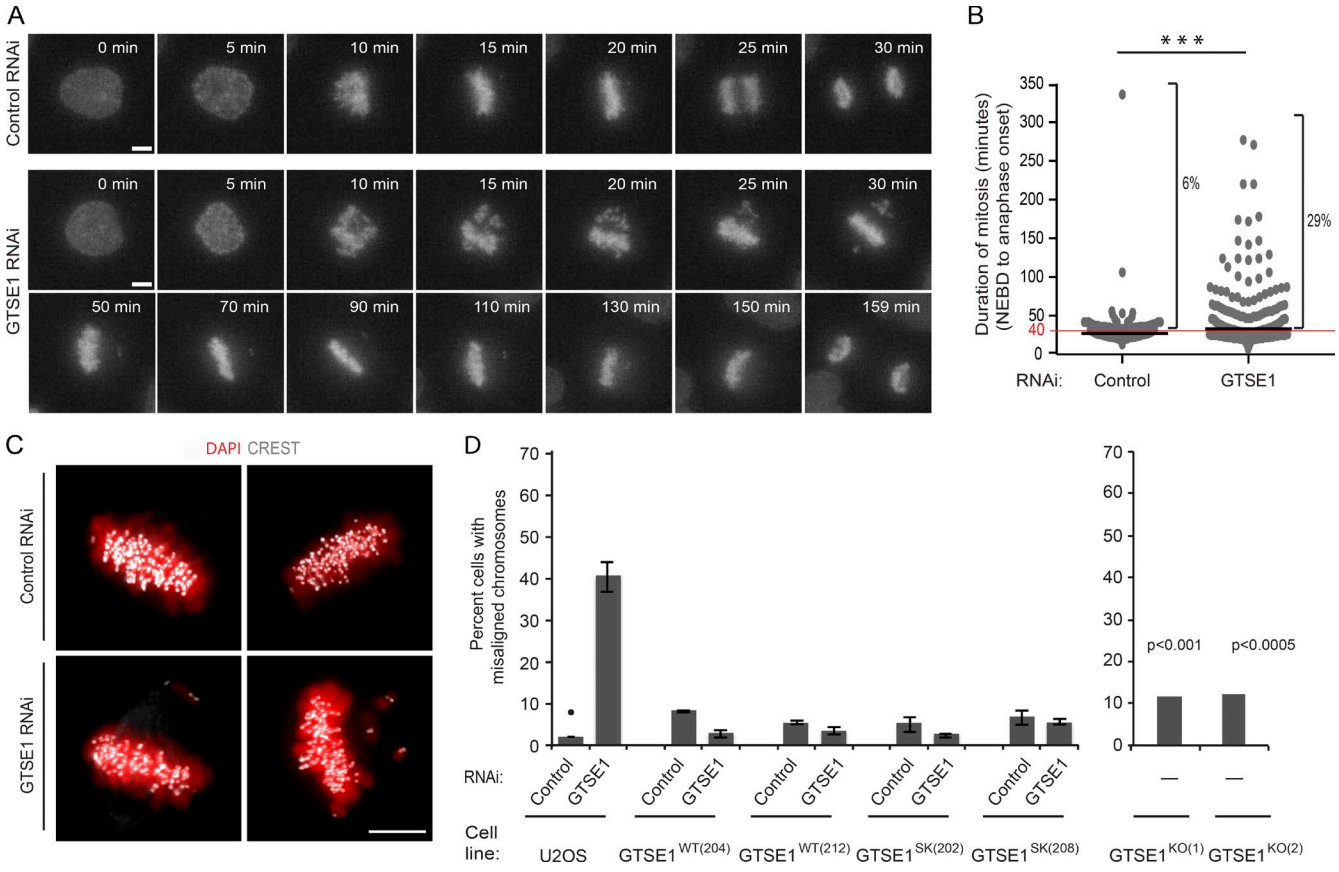

Figure 2. **GTSE1 is required for efficient chromosome alignment.** (A) Still frames of mitoses from time-lapse videos (Videos 1 and 2) of U2OS cells expressing histone H2AFZ-mCherry after control (top row) or GTSE1 RNAi (bottom two rows). GTSE1-depleted cells require a longer time to align all chromosomes and enter anaphase. (B) Mitotic duration (nuclear envelope breakdown [NEBD] to anaphase onset) of individual cells is plotted from the analysis of videos of control or GTSE1 RNAi-treated U2OS histone H2AFZ-mCherry cells as are shown in A. GTSE1-depleted cells have a longer mean duration of mitosis (control RNAi: 28.4 ± 20.5 min, n = 269; GTSE1 RNAi: 42.5 ± 36.3 min, n = 295; black bars represent the mean) and a higher percentage of cells with mitotic durations longer than 40 min (5.9% of control-depleted cells vs. 29.2% of GTSE1-depleted cells). (C) Immunofluorescence images of chromosomes (red) and kinetochores (white) in fixed U2OS cells after control or GTSE1 RNAi. (D) Quantification of the percentage of cells with misaligned chromosomes from immunofluorescence analysis as shown in C. The left graph shows control or GTSE1 RNAi of U2OS cells, two stable U2OS cell clones expressing RNAi-resistant GTSE1 ($GTSE1^{WT(204)}$ and $GTSE1^{WT(212)}$), and two stable U2OS cell clones expressing RNAi-resistant GTSE1 mutated to abolish interaction with EB1 ($GTSE1^{Sk(202)}$ and $GTSE1^{Sk(208)}$). n > 150 cells; 3 experiments per condition. The right graph shows two independent U2OS GTSE1 knockout clones. P-values were obtained from a χ^2 test comparing against the U2OS control condition (marked with •). n > 100 cells. Error bars represent SEM. Bars, 5 µm. ***, $P \leq 0.001$.

spindle axis within 20° relative to the surface (Fig. 1 H). Thus, GTSE1 is necessary for the stabilization of MTs in mitosis and for proper spindle orientation.

GTSE1 is required for efficient chromosome alignment

To determine whether GTSE1 plays a role in mitotic progression and chromosome segregation, we imaged live U2OS cells expressing histone mH2A.Z-mCherry progressing through mitosis after RNAi (Figs. 2 A and S1 C and Videos 1 and 2). GTSE1-depleted cells took significantly longer than control-depleted cells to align all of their chromosomes and enter anaphase (control RNAi: 28.4 ± 20.5 min; GTSE1 RNAi: 42.5 ± 36.3 min; Fig. 2 B). To quantify the chromosome alignment defect, we fixed cells after RNAi and determined the percentage of cells containing misaligned chromosomes but otherwise displaying a metaphase-like morphology (Fig. 2, C and D). Approximately 40% of GTSE1-depleted cells contained misaligned chromosomes, and this defect was rescued by expression of a wild-type RNAi-resistant GTSE1-GFP transgene, as well as the SxIP-mutated transgene, confirming the specificity of GTSE1 RNAi (Fig. 2 D). Misaligned chromosomes were also significantly increased in both $GTSE1^{KO}$ cell lines, although to a lesser extent, suggesting these cell lines may be adapted through selection of a genetic (or epigenetic) alteration that increases the fidelity of chromosome segregation and viability in a GTSE1 knockout background. We analyzed protein levels of several mitotic regulators related to MT dynamics and GTSE1 function in these knockout cells but did not see differences in wild-type cells (Fig. S2, B and F–H).

GTSE1 stabilizes kinetochore–MT attachment

The defect in chromosome alignment and delay in anaphase onset in GTSE1-depleted cells indicated that the spindle assembly checkpoint was active in these cells and suggested that they may be compromised for their ability to establish proper and stable kinetochore–MT attachments. To more specifically analyze this, we first quantified the abundance of MAD1, which is recruited to kinetochores that do not have proper kinetochore–MT attachments (Howell et al., 2004), in metaphase cells with aligned chromosomes. Indeed, GTSE1-depleted metaphase cells displayed increased kinetochore localization of MAD1

(Fig. 3 A). The delays in chromosome alignment and MAD1 persistence at kinetochores after GTSE1 depletion could arise from the destabilization of MTs and of kinetochore–MT attachments. To determine whether GTSE1 was required specifically for the stability of kinetochore MTs, we first tested whether there was a reduction in the cold-stable kinetochore MT population of metaphase cells after GTSE1 depletion. Indeed, GTSE1-depleted cells had a significant reduction of cold-stable kinetochore MTs as compared with control-treated cells (Fig. 3 B). To quantify kinetochore MT stability, we then assayed kinetochore MT turnover by measuring loss of fluorescence after photoactivation in metaphase U2OS cells expressing photoactivatable (PA) GFP-tubulin (Zhai et al., 1995; Bakhoum et al., 2009b). Analysis of fluorescence dissipation after photoactivation (FDA PA) indicated that cells depleted of GTSE1 showed a decrease in the half-life of kinetochore MTs as compared with control RNAi (Figs. 3 C, S1 D, and S3 A), indicating a reduction in the stability of kinetochore–MT attachments. Consistent with a role in stabilizing kinetochore MTs, we observed that GTSE1 localized to kinetochore MTs, as visualized by removing nonkinetochore MTs by cold treatment and staining for GTSE1 and kinetochores (Fig. 3 D and Videos 3 and 4). Collectively, these results implicate GTSE1 as an important regulator of MT stability in mitosis that is necessary to stabilize kinetochore–MT attachment and promote efficient alignment of chromosomes.

Mitotic defects after GTSE1 depletion are dependent on the activity of MCAK

We next asked what the mechanism is by which GTSE1 promotes MT stability in mitosis. GTSE1 is highly phosphorylated when cells enter mitosis and does not associate directly with growing MT tips nor with the MT lattice (Scolz et al., 2012; and unpublished data), indicating that the stabilizing effect of GTSE1 on MTs in mitosis is mediated through other protein interactors. We previously showed that GTSE1 interacts with a complex containing TACC3 (Hubner et al., 2010), which has also been implicated in controlling MT stability (Kinoshita et al., 2005; Lin et al., 2010; Booth et al., 2011; Cheeseman et al., 2013; Nixon et al., 2015). We did not, however, detect a significant change in TACC3 localization to MTs in GTSE1-depleted cells nor in GTSE1 knockout cell lines (Fig. S3 B), consistent with our earlier study (Hubner et al., 2010). Analysis of mitotic interactors of GTSE1 from our previous immunoprecipitation and mass spectrometry results (Hubner et al., 2010) revealed that the MT depolymerase MCAK (Kif2C) was also consistently enriched across repeated experiments. We confirmed this interaction in cells by immunoprecipitating either endogenous or stably BAC-expressed GFP-tagged GTSE1 from mitotic cells and probing with antibodies against MCAK (Fig. 4, A and B).

The perturbed mitotic phenotypes after GTSE1 depletion (loss of MT stability and chromosome alignment defects) are reminiscent of the reported mitotic phenotypes upon increasing MCAK activity via overexpression (Maney et al., 1998; Moore and Wordeman, 2004; Zhang et al., 2011), suggesting that GTSE1 may normally attenuate MCAK activity, which becomes unregulated and hyperactive upon loss of GTSE1. We reasoned that if the loss of MT stability in mitosis after GTSE1 depletion resulted from excessive MCAK activity, then reducing MCAK levels/activity in these cells should restore MT stability. To test this, we depleted GTSE1 and MCAK by RNAi either individually or together and imaged mitotic cells by immunofluorescence (Figs. 4 C and S1, E and F). RNAi of MCAK alone in U2OS cells strongly decreased MCAK protein levels and led to an increase in mitotic cells containing longer, curved, and more dense astral MTs, consistent with previous studies (Rizk et al., 2009; Rankin and Wordeman, 2010). When MCAK was co-depleted from cells with GTSE1, in contrast to GTSE1 depletion alone, most cells displayed abundant, long astral MTs, indicating that the loss of MT stability observed after GTSE1 depletion is dependent on MCAK activity (Fig. 4, C–E). MT intensity within the inner spindle regions also increased after co-depletion of GTSE1 and MCAK as compared with GTSE1 alone, indicating that the MCAK dependency of GTSE1 depletion phenotypes was not specific to astral MTs (Fig. 4 F). Because astral MTs are known to mediate spindle orientation (Pearson and Bloom, 2004), we asked whether the spindle orientation defect that occurred after GTSE1 RNAi was restored after MCAK co-depletion as well. Indeed, the spindle orientation defect after GTSE1 RNAi was also dependent on MCAK (Fig. 4 G). If the defects in chromosome alignment seen upon depletion of GTSE1 resulted from MCAK-mediated defects in MT stability, we expected they would also be ameliorated by co-depletion of MCAK. Remarkably, upon co-depletion of GTSE1 and MCAK, there was a dramatic reduction in misaligned chromosomes as compared with GTSE1 RNAi alone (Fig. 4 H).

These results show that all observed mitotic phenotypes associated with the depletion of GTSE1 are alleviated by co-depletion of MCAK. The same effect was seen when MCAK was depleted in GTSE1^{KO} cells (Fig. S2 I). This alleviation was specific to MCAK, as co-depletion of the related kinesin-13 MT depolymerase Kif2A with GTSE1 did not restore MT stability nor chromosome alignment (Figs. S1 G and S3 C). Furthermore, although total MCAK protein levels were unchanged after loss of GTSE1 (Fig. S1 H), MCAK localization to the spindle is abnormal (Fig. 4 I). Collectively, these findings indicate that GTSE1 functions to negatively regulate MCAK MT depolymerase activity to ensure the stability of MTs required for spindle orientation and chromosome alignment throughout the spindle.

GTSE1 interacts directly with MCAK and inhibits its MT depolymerase activity in vitro

To determine the mechanism by which GTSE1 antagonizes MCAK activity, we first asked whether we could detect a direct interaction of MCAK with a defined domain of GTSE1. We performed in vitro pull-down assays with purified MCAK and either a purified GST-tagged GTSE1 N-terminal fragment containing residues 1–460 or a C-terminal fragment containing residues 463–739, the latter of which contains the regions of GTSE1 previously identified to interact with EB1 (Scolz et al., 2012) and p53 (Monte et al., 2003). The N-terminal fragment abundantly pulled down purified MCAK protein, whereas the C-terminal fragment did not (Figs. 5 A and S4 A), indicating that GTSE1 binds to MCAK via the N-terminal half of the protein.

To test whether GTSE1 could inhibit MCAK activity in vitro, we purified full-length GTSE1 and MCAK from insect cells (Fig. S4, B–D) and assayed the MT depolymerase activity of MCAK on labeled MTs using total internal reflection fluorescence (TIRF) microscopy (Helenius et al., 2006). Addition of MCAK alone to GMPCPP-stabilized MTs resulted in rapid MT depolymerization (Fig. 5 B and Video 5). Addition of either equimolar or fivefold excess amounts of GTSE1 protein to this reaction completely eliminated MCAK-induced depolymerization (Fig. 5 B and Video 6). This was not caused by an inherent

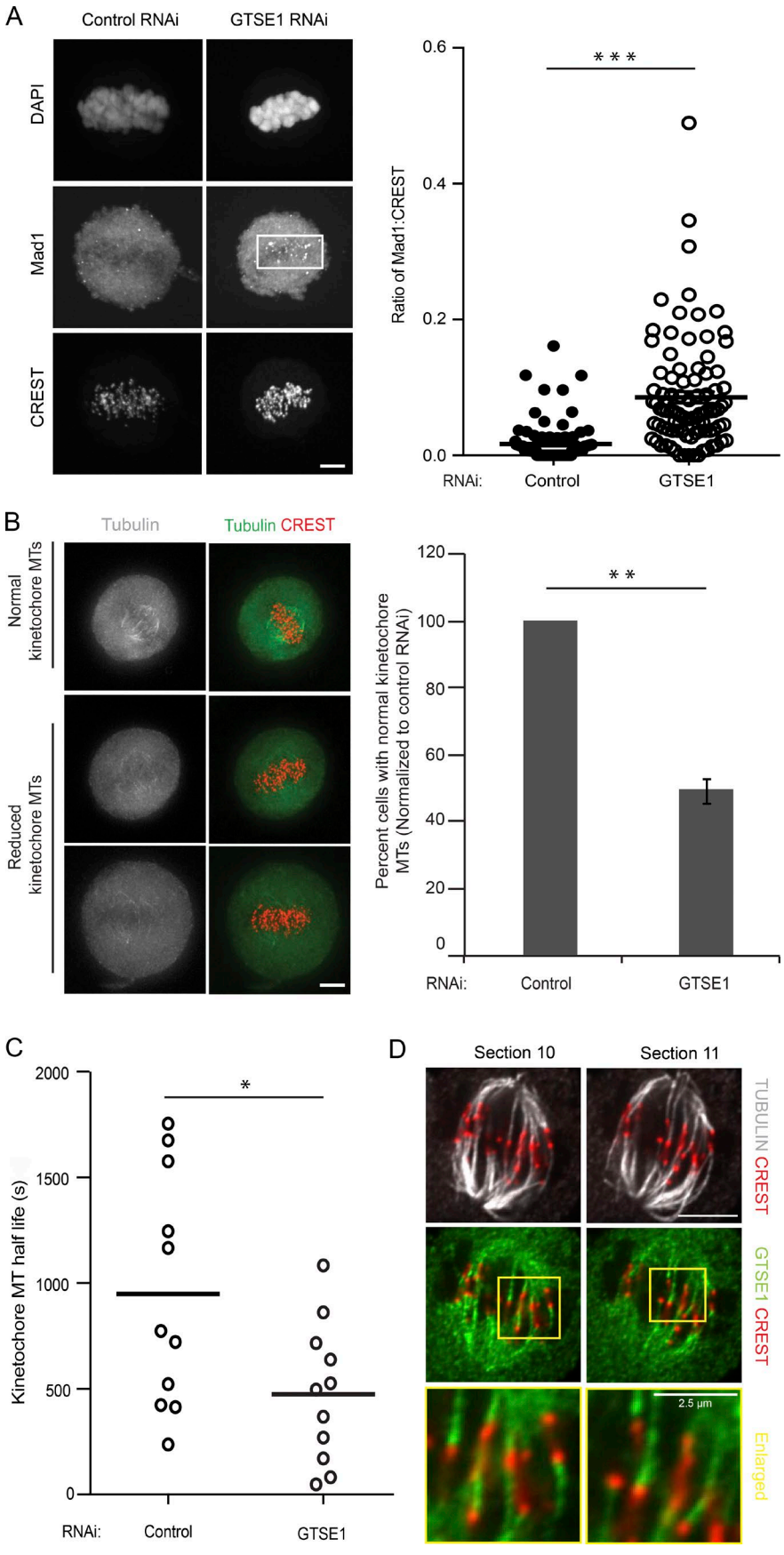

Figure 3. **GTSE1 localizes to kinetochore MTs and stabilizes kinetochore–MT attachments.** (A) Representative immunofluorescence images of metaphase U2OS cells stained with DAPI (DNA), MAD1, and CREST showing MAD1 accumulation on kinetochores after GTSE1 RNAi. Cells were blocked using Cdk1 inhibitor (RO-3306) and released for 1 h in normal media to enrich the number of metaphase mitotic cells. The white box indicates the region with Mad1-positive kinetochores. $n > 90$ cells; 3 independent experiments. (B) Fewer GTSE1-depleted cells contain cold-stable MTs than control-depleted cells. Images show mitotic cells fixed after cold treatment and stained for tubulin and kinetochores. The graph shows the proportion of cells containing a full complement of cold-stable MTs after cold treatment, after control cells were normalized to 100%. The cells were blocked using Cdk1 inhibitor (RO-3306) and released for 1 h in normal media to enrich the number of metaphase mitotic cells. $n > 100$ cells per experiment; 3 experiments per condition. (C) Graph showing kinetochore MT half-life in control or GTSE1-depleted U2OS cells expressing PA GFP-tubulin (Fig. S3). Each circle represents the kinetochore MT half-life of a single cell; bars represent the mean. $n = 11$ cells; 3 experiments per condition. (D) Representative immunofluorescence images (slices 10 and 11 from Videos 3 and 4) showing GTSE1 decorating K-fibers in U2OS cells expressing BAC-based GTSE1-LAP after cold treatment. The cells were stained for GTSE1, kinetochores (CREST), and MTs (tubulin). All error bars represent SEM. Bars, 5 µm (unless stated otherwise). *, $P \leq 0.05$; **, $P \leq 0.01$; ***, $P \leq 0.001$.

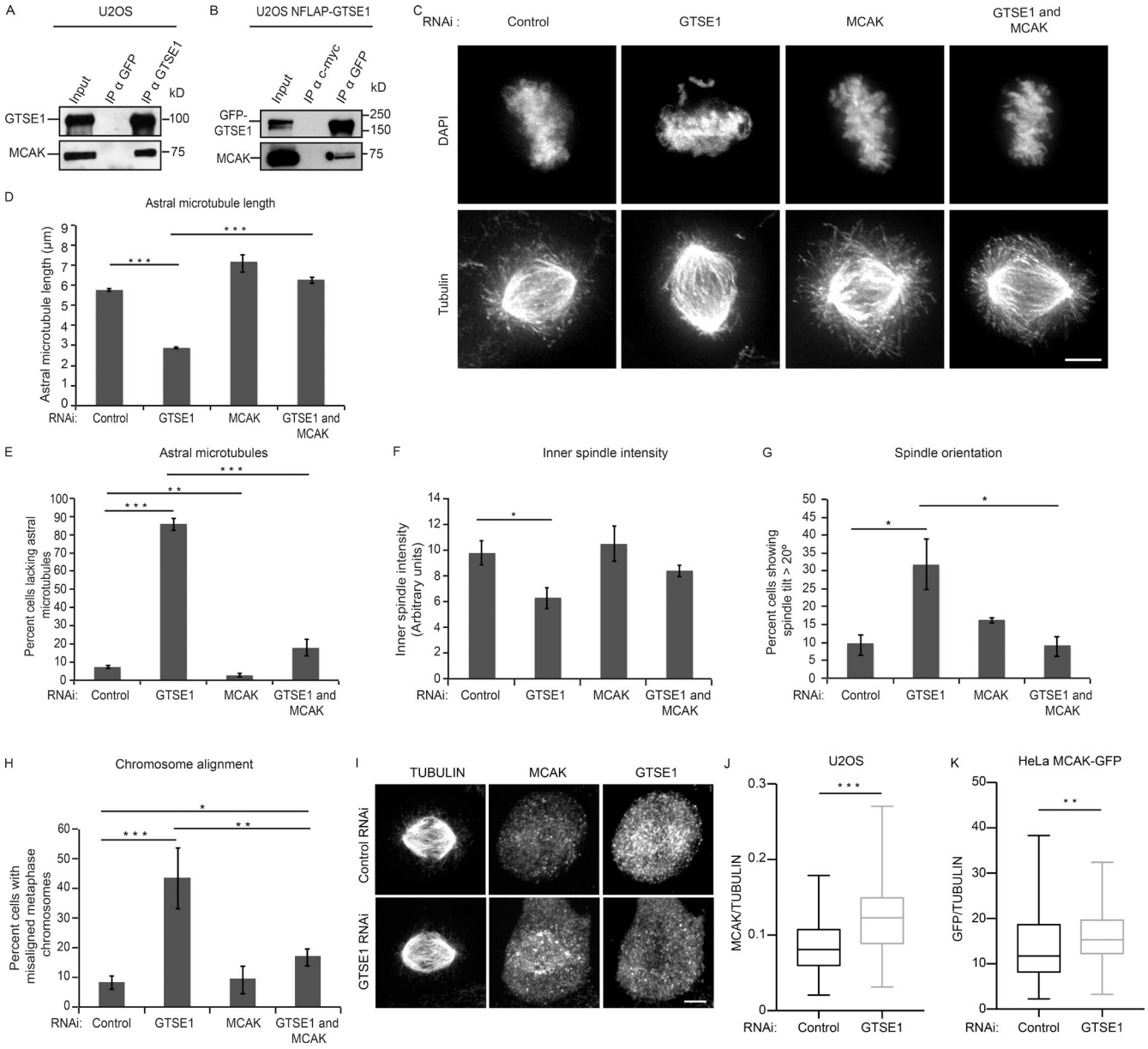

Figure 4. **Mitotic defects after GTSE1 depletion are dependent on the activity of the MT depolymerase MCAK.** (A) MCAK coimmunoprecipitates with GTSE1. Western blot after immunoprecipitation (IP) from U2OS cell lysates using either anti-GTSE1 or anti-GFP antibodies and probing with anti-GTSE1 or anti-MCAK antibodies. (B) Western blot after immunoprecipitation from U2OS NFLAP-GTSE1 cell lysates using either anti-GFP or anti–c-myc antibodies and probing with anti-GFP or anti-MCAK antibodies. (C) Immunofluorescence images of mitotic U2OS cells after control, GTSE1, MCAK, or combined GTSE1 and MCAK RNAi, stained for DNA (DAPI) and MTs (tubulin). (D) Quantification of the mean length of astral MTs in three dimensions from immunofluorescence analysis as shown in C. 10 astral MTs were measured per cell. n = 10 cells per experiment; 3 experiments per condition. (E) Quantification of the percentage of cells lacking astral MTs from immunofluorescence analysis as shown in C. n > 100 cells per experiment; 3 experiments per condition. (F) Quantification of inner spindle tubulin fluorescence intensity from immunofluorescence analysis as shown in C. $n \geq 19$ per experiment; 3 experiments per condition. (G) Analysis of spindle orientation. Quantification of the percentage of metaphase cells with a spindle tilt angle of >20° is shown for each RNAi condition. n > 140 cells; 4 experiments per condition. (H) Quantification of the percentage of cells with misaligned chromosomes from immunofluorescence analysis as shown in C. n > 100 cells per experiments; 3 experiments per condition. (I) Immunofluorescence images of mitotic U2OS cells showing MCAK localization after control and GTSE1 RNAi. Cells were stained for MCAK, GTSE1, and MTs (tubulin). (J) Quantification of MCAK intensity on the inner spindle normalized to tubulin intensity in U2OS cells using immunofluorescence images after control and GTSE1 RNAi. $n \geq 105$ cells; 3 independent experiments. P-values were obtained using a Mann-Whitney U test. (K) Quantification of MCAK intensity using GFP fluorescence on the inner spindle normalized to tubulin intensity in HeLa cells expressing BAC-based MCAK-GFP using immunofluorescence images after control and GTSE1 RNAi. $n \geq 89$ cells; 3 independent experiments. P-values were obtained using a Mann-Whitney U test. Bars, 5 μm. All error bars represent SEM. *, $P \leq 0.05$; **, $P \leq 0.01$; ***, $P \leq 0.001$.

ability of GTSE1 to stabilize MTs because GTSE1 does not have the same impact on MCAK-independent MT depolymerization. We could only detect a minimal reduction in the MT shrinkage rate after catastrophe when GTSE1 alone was added at the higher concentration to dynamic MTs, and catastrophe frequency was not reduced (Fig. 5 C and not depicted). Consistently, we also observed a concentration-dependent inhibition of MCAK depolymerase activity using taxol-stabilized MTs

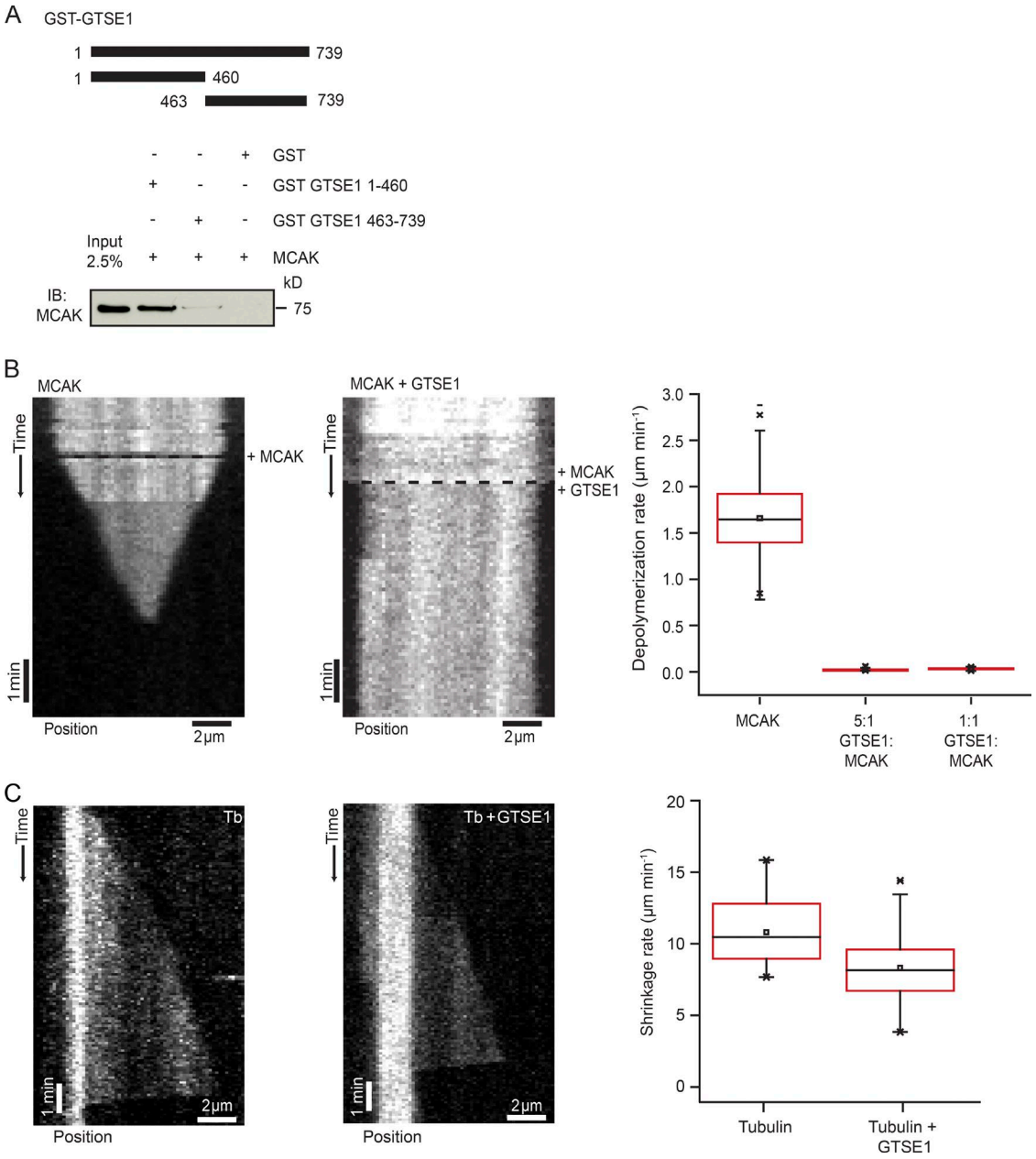

Figure 5. **GTSE1 interacts directly with MCAK and inhibits its MT depolymerase activity in vitro.** (A) Immunoblot (IB) showing MCAK pulled down in an in vitro GST pulldown using GST alone, GST-GTSE1 1–460, and GST-GTSE1 463–739 fragments. Input represents 2.5% of total MCAK protein used for the GST pulldown assay. (B) Kymograph depicting 50 nM MCAK depolymerizing a GMPCPP-stabilized MT (Video 5). The black dashed line represents the start of the experiment when MCAK was added. The second kymograph depicts a GMPCPP-stabilized MT maintaining constant length in the presence of 50 nM MCAK plus 250 nM GTSE1 (Video 6). The black dashed line represents the start of the experiment when MCAK and GTSE1 were added. Depolymerization rates of GMPCPP-stabilized MTs in the presence of 50 nM MCAK alone, 50 nM MCAK with a fivefold excess of GTSE1, and 50 nM MCAK with an equimolar amount of GTSE1 are shown in the box plot. $n > 100$ MTs; 4 experiments. (C) Kymographs of MT growth and catastrophe in the presence of 20 µM tubulin (Tb) alone or 20 µM tubulin and 250 nM GTSE1 from GMPCPP-MT seeds. Box plot shows the shrinkage rate after catastrophe of 20 µM tubulin alone and 20 µM tubulin with 250 nM GTSE1. $n = 34$ and 90 MTs, respectively.

and decreasing amounts of GTSE1 protein in bulk MT sedimentation assays (Fig. S4 E; Desai et al., 1999). Thus, GTSE1 inhibits MCAK depolymerization activity in vitro.

Depleting GTSE1 reduces chromosome missegregation frequency in CIN cancer cell lines

Overexpression of MCAK in CIN cancer cell lines reduces kinetochore–MT attachment hyperstability, thereby allowing correction of erroneous merotelic kinetochore–MT attachments and decreasing the rate of chromosome missegregation and CIN (Bakhoum et al., 2009b). Because GTSE1 is a negative regulator of MCAK activity and has up-regulated protein levels in several cancer cell lines and tumors relative to nontransformed cells (Scolz et al., 2012), we wondered whether GTSE1 expression in these cells contributed to CIN. First, we analyzed anaphase chromosome segregation defects, including lagging chromosomes, which correlate with CIN (Thompson and Compton,

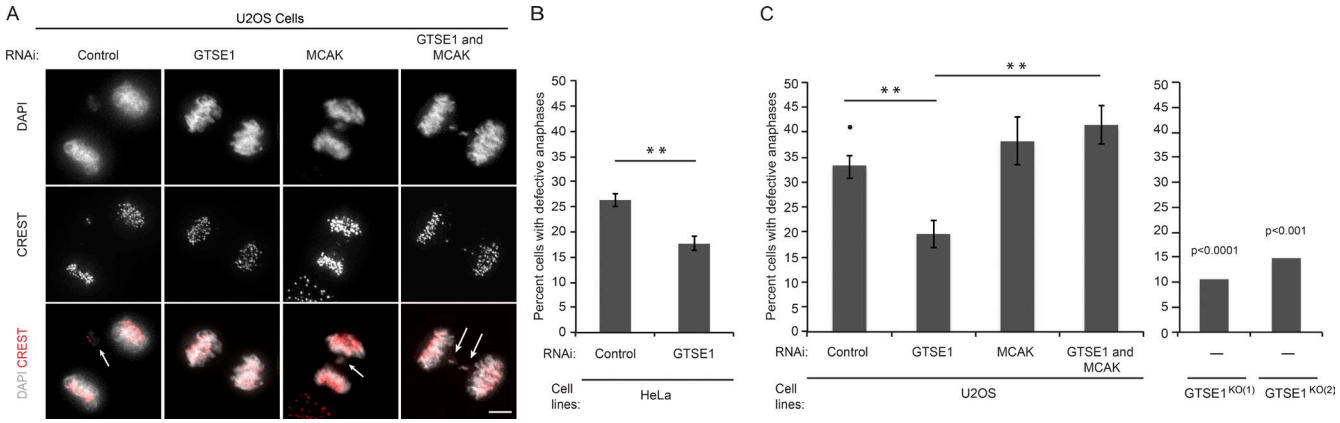

Figure 6. **Reduction of GTSE1 levels reduces anaphase chromosome segregation defects in HeLa and U2OS cells.** (A) Immunofluorescence images of anaphase U2OS cells after control, GTSE1, MCAK, or GTSE1 and MCAK siRNA stained for DNA (DAPI) and kinetochores (CREST). White arrows indicate anaphase segregation defects. (B) Quantification of the percentage of anaphase HeLa cells with defective anaphase chromosome segregation events. $n > 390$ per condition; 3 experiments. (C) Quantification of the percentage of anaphase U2OS cells with defective anaphase chromosome segregation events from immunofluorescence analysis as shown in A. The left graph shows U2OS cells after RNAi conditions as in A. $n > 65$ per experiment; 3 experiments per condition. The right graph shows two independent U2OS GTSE1 knockout clones. P-values were obtained from a χ^2 test comparing against the U2OS control condition (marked with •). $n > 100$ cells. **, $P \leq 0.01$.

2008; Bakhoum et al., 2014). In HeLa and U2OS cells, highly CIN cancer cell lines with high levels of GTSE1 protein, we found that reduction of GTSE1 levels by RNAi significantly reduced the frequency of anaphase chromosome segregation defects (Fig. 6, A–C). Remarkably, both U2OS cell lines with GTSE1 stably knocked out showed an even greater reduction in the frequency of anaphase chromosome segregation defects (Fig. 6 C). Closer analysis of GTSE1-depleted cells revealed that the reduction in anaphase chromosome segregation defects could be attributed specifically to lagging chromosomes, which generally arise from merotelic attachments, as opposed to chromosome bridges or acentric fragments (Fig. S5). Importantly, this impact of GTSE1 on chromosome missegregation is also mediated through MCAK, as reducing GTSE1 levels in cells also depleted of MCAK did not have an effect on the frequency of anaphase chromosome segregation defects (Fig. 6 C).

Elevating GTSE1 levels induces chromosome missegregation and CIN

We next asked whether overexpression of GTSE1 induced anaphase chromosome segregation defects in HCT116 cells, which are near-diploid, relatively chromosomally stable, and have relatively low levels of GTSE1 protein (Fig. 7 A; Thompson and Compton, 2008). We stably transfected HCT116 and HCT116 p53$^{-/-}$ cells with a GTSE1-GFP cDNA construct that allowed us to maintain cells overexpressing GTSE1 over many generations through antibiotic selection (Fig. 7, A and B). We isolated clonal transformants overexpressing GTSE1-GFP ~3–10-fold higher than nontransfected cells and grew them for ~60 generations before analyzing mitotic cells. Although these cells displayed an ~30% increase in MT density, no major morphological changes to the spindle were observed, and relative TACC3 recruitment to MTs did not increase (Fig. S3 D). All HCT116 cell clones overexpressing GTSE1 did, however, show a significant increase in the frequency of anaphase chromosome segregation defects (Fig. 7, C and D).

Finally, we asked whether increased levels of GTSE1 in HCT116 cells would induce CIN in these cells. Clonal cell lines overexpressing GTSE1 were analyzed for the frequency with which cells contained deviations from the disomic state after ~60 generations by FISH analysis of chromosomes 7 and 11 (Fig. 8 A), as compared with mock-transfected clones. Independent HCT116 clones overexpressing GTSE1-GFP displayed a significant increase in cells containing deviations from the disomic state (Fig. 8, B–D). As p53 has been reported to induce apoptosis after chromosome missegregation (Thompson and Compton, 2008), we also performed these experiments in HCT116 p53$^{-/-}$ cells, which also showed elevated frequencies of anaphase segregation defects after GTSE1 overexpression (Fig. 7 D). HCT116 p53$^{-/-}$ clones overexpressing GTSE1-GFP displayed a yet greater increase in deviations from the modal number of chromosomes as compared with mock-transfected clones (Fig. 8, B, E, and F). Thus, reduction of GTSE1 levels in highly CIN cancer cell lines reduces the frequency of lagging chromosomes, whereas overexpression of GTSE1 in chromosomally stable cell lines induces lagging chromosomes and whole chromosome CIN.

Discussion

Here, we have demonstrated that GTSE1 regulates MT stability by inhibiting MCAK MT depolymerase activity. Depletion of GTSE1 enhances MCAK activity in mitotic cells to levels that are incompatible with the stabilization of astral MTs and kinetochore–MT interactions, leading to defects in spindle positioning and chromosome capture and alignment. At the same time, GTSE1 depletion results in fewer chromosome segregation defects in the cancer cell lines tested, consistent with the decreased stability of kinetochore–MT interactions enhancing the ability to correct merotelic attachments. Remarkably, knocking out GTSE1 in U2OS cancer cells resulted in stable cell lines with dramatically reduced missegregation frequencies. Whereas these knockout cell lines also displayed decreased MT stability similar to that observed after RNAi-mediated depletion of GTSE1, they did not exactly phenocopy siRNA-depleted cells; in knockout cells, chromosome misalignment was less severe. Because the BAC transgene rescue experiments (Figs. 1 B and 2 D) ruled out off-target siRNA effects, it appears that this difference in the knockout cells reflects either a long-term

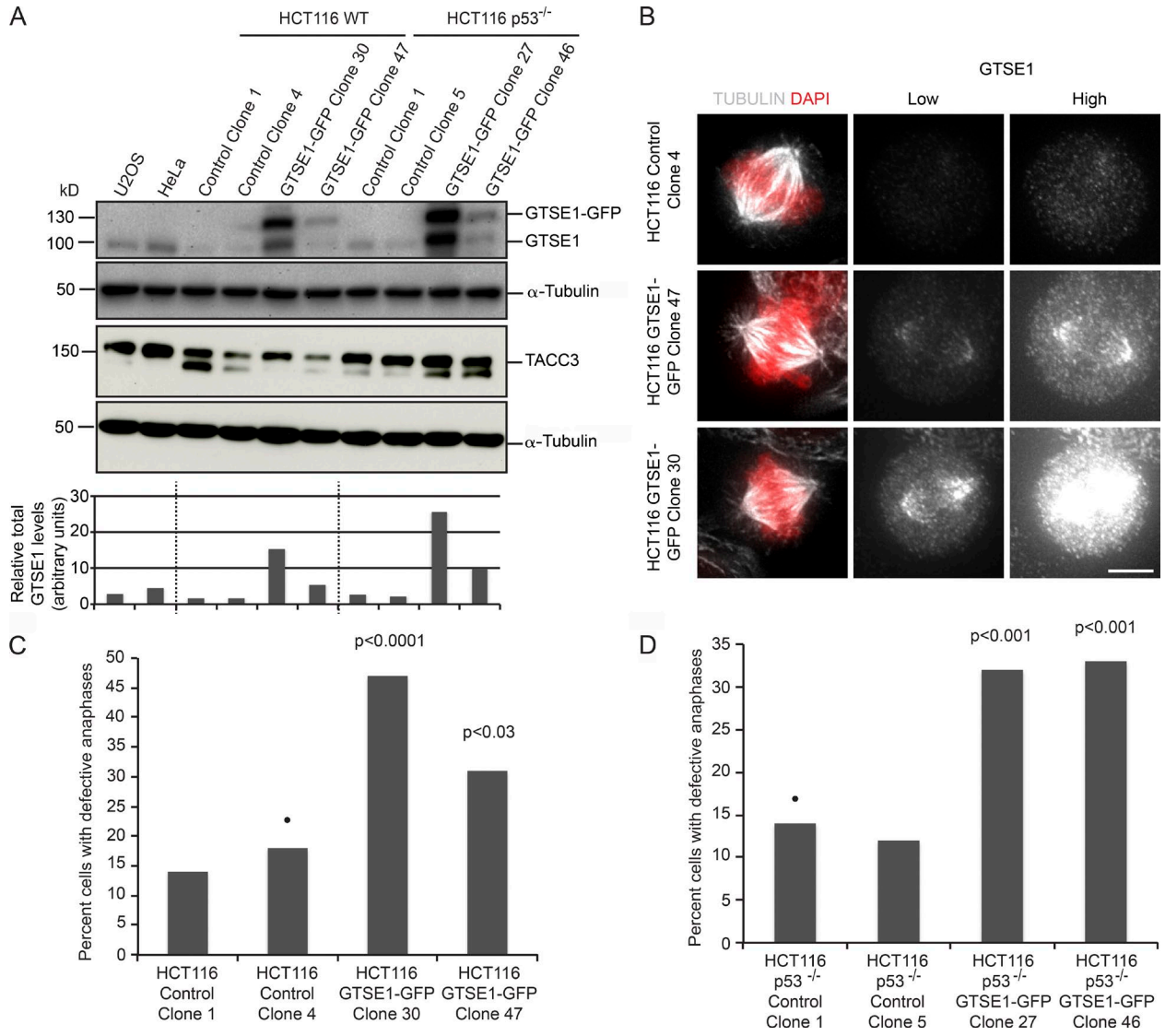

Figure 7. **Overexpression of GTSE1 induces segregation defects in HCT116 cells.** (A) Representative Western blots of cell lysates from U2OS, HeLa, and HCT116 and HCT116 p53$^{-/-}$ control and GFP-GTSE1–expressing clonal cell lines used for analysis in C and D. Blots were probed with anti-GTSE1, anti-TACC3, and anti–α-tubulin. The graph represents quantification of GTSE1 protein levels normalized to tubulin levels from the blot shown. The relative abundance of total GTSE1 protein was quantified and normalized to tubulin levels. (B) Low and high intensity immunofluorescence images of HCT116 control and GTSE1-GFP–overexpressing clones showing normal spindle morphology stained for DNA (DAPI), GTSE1, and MTs (tubulin). (C) Quantification of the percentage of anaphase cells with lagging chromosomes for control or GTSE1-GFP–expressing HCT116 clones. $n \geq 99$. (D) Quantification of the percentage of anaphase cells with lagging chromosomes for control or GTSE1-GFP–expressing HCT116 p53$^{-/-}$ clones. $n \geq 104$. P-values were obtained from χ^2 tests comparing control clones (designated by •). Bar, 5 µm. **, $P \leq 0.01$.

GTSE1-loss phenotype or that clones have been adapted though selection to tolerate loss of GTSE1 by suppressing the chromosome misalignment defect. Of note, we did not observe reduction in MCAK protein levels in these cells, and the dependency of the perturbed phenotypes on MCAK remained.

The precise regulation of MCAK activity is essential for several cellular processes that rely on dynamic MTs (Maney et al., 1998; Walczak et al., 2002; Kline-Smith et al., 2003; Lan et al., 2004; Rankin and Wordeman, 2010; Domnitz et al., 2012; Braun et al., 2014). The potent MT depolymerase activity of MCAK observed in vitro suggests that its activity must be generally repressed in cells. This may allow for precise spatial and temporal activation of its activity for discrete functions. Here, we have elucidated a novel regulatory mechanism responsible for the inhibition of MCAK activity through interaction with GTSE1. In vitro, GTSE1 protein present at equimolar amounts to MCAK is sufficient to completely inhibit MCAK depolymerase activity, suggesting GTSE1 may be a target for the differential regulation of MCAK activity in cells.

Most proposed mechanisms to date for the direct inhibition of MCAK activity involve phosphorylation of MCAK and/or intramolecular rearrangements (Ems-McClung et al., 2013; Burns et al., 2014; Talapatra et al., 2015). Several phosphorylation sites dependent on multiple mitotic kinases identified on MCAK have been shown to be required for both positive and negative modulation of its activity (Andrews et al., 2004; Lan et al., 2004; Zhang et al., 2007, 2011; Sanhaji et al., 2010; Tanenbaum et al., 2011; Ems-McClung et al., 2013), but how these various phosphorylation events control MCAK activity in the cellular context remain largely unknown. It was recently shown

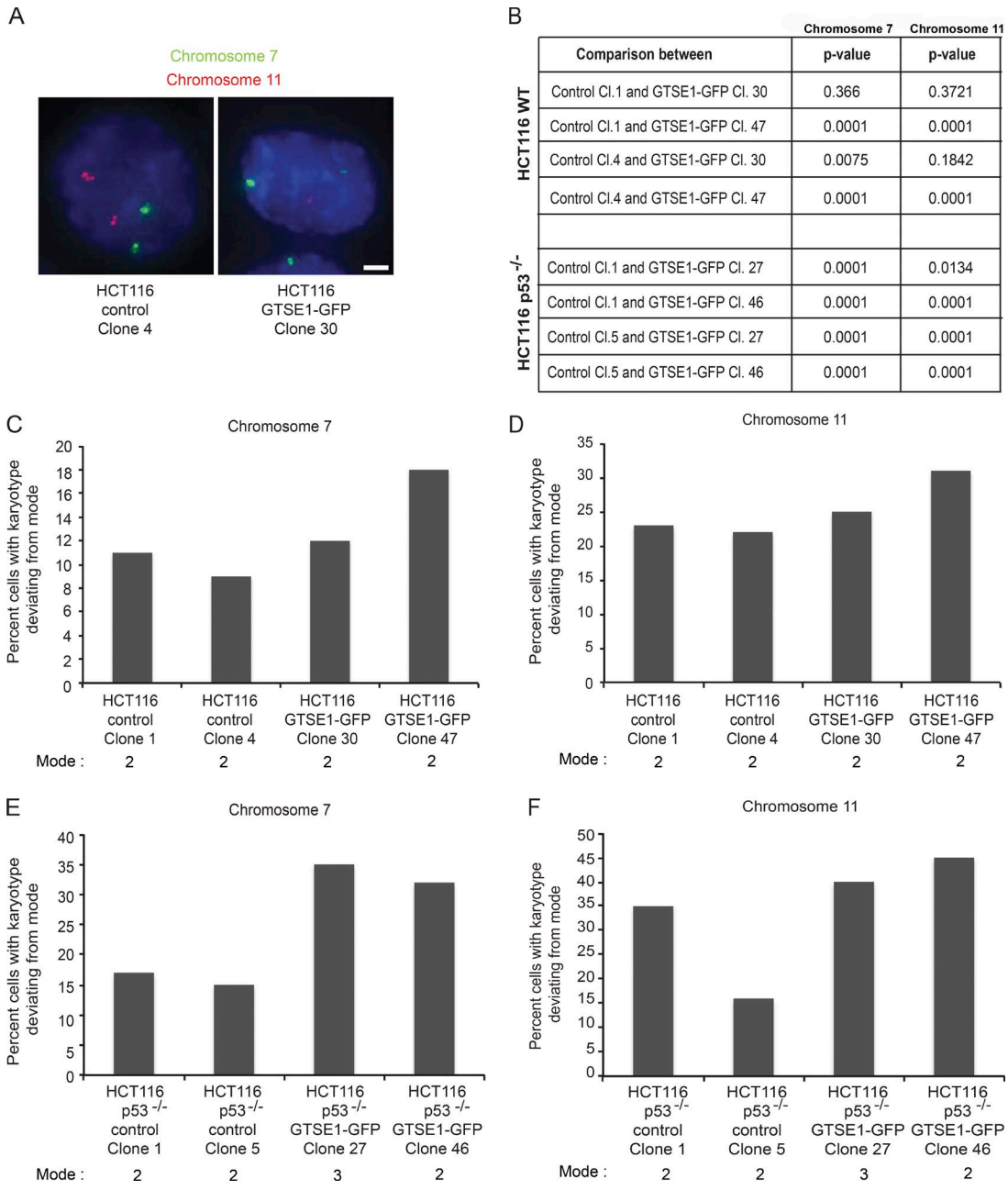

Figure 8. **Overexpression of GTSE1 induces CIN in HCT116 cells.** (A) Fluorescence images from fixed control or GTSE1-GFP–overexpressing clonal HCT116 cells processed for FISH. Probes for α-satellite regions on chromosomes 7 (green) and 11 (red) are shown and were used to count the number of copies of each chromosome in cells. Bar, 5 µm. (B) Statistically significant values from comparing deviances from the modal number of chromosomes in control versus GTSE1-GFP–overexpressing HCT116 cells from data presented in C–F. P-values were determined from χ^2 analysis comparing the indicated clonal cell lines. (C) Percentage of HCT116 control or GFP-GTSE1–expressing clonal cell lines containing numbers of chromosome 7 deviating from the mode. $n > 980$ cells for each condition. (D) Percentage of HCT116 control or GFP-GTSE1–expressing clonal cell lines containing numbers of chromosome 11 deviating from the mode. $n > 980$ cells for each condition. (E) Percentage of HCT116 p53$^{-/-}$ control or GFP-GTSE1–expressing clonal cell lines containing numbers of chromosome 7 deviating from the mode. $n > 1{,}000$ cells for each condition. (F) Percentage of HCT116 p53$^{-/-}$ control or GFP-GTSE1–expressing clonal cell lines containing numbers of chromosome 11 deviating from the mode. $n > 1{,}000$ cells for each condition.

that nucleolar spindle-associated protein modulation of MCAK activity is dependent on Aurora B phosphorylation (Li et al., 2016). It will be interesting in the future to determine whether GTSE1 association with MCAK is regulated by, or influences, MCAK's phosphorylation state. A conformation of MCAK where the C-terminal tail interacts with its motor/neck domain is emerging as an important transition state during its catalytic cycle, and this transition could be a target for controlling its cellular regulation (Ems-McClung et al., 2013; Talapatra et al., 2015; Zong et al., 2016). Indeed, phosphorylation by Aurora B has been shown to affect this conformation in vitro (Ems-McClung et al., 2013). Furthermore, it was recently shown that point mutations in MCAK impairing this conformation lead to increased MCAK activity toward MTs as a result of enhanced accumulation of MCAK at the spindle poles, reminiscent of what we observe after GTSE1 depletion (Fig. 4 I; Zong et al.,

2016). Determining the impact of GTSE1 interaction with MCAK on its ability to transition between distinct conformational states will be informative.

Our finding that GTSE1 regulates MT stability is interesting to consider in the context of Aurora A kinase control of MT stability. Aurora A kinase activity controls GTSE1 localization to the spindle (Hubner et al., 2010). During mitosis, Aurora A phosphorylates the TACC3 protein, which allows TACC3 to interact with clathrin heavy chain, forming an MT interaction interface that brings the pTACC3–clathrin complex to the spindle (Kinoshita et al., 2005; Fu et al., 2010; Hubner et al., 2010; Lin et al., 2010; Booth et al., 2011; Hood et al., 2013). GTSE1 spindle localization is dependent on Aurora A, TACC3, and clathrin, and GTSE1 is the most downstream of these components recruited to the spindle (Hubner et al., 2010). Loss of Aurora A, TACC3, or clathrin, like GTSE1, results in defects in MT stability and chromosome alignment (Giet et al., 2002; Marumoto et al., 2003; Bird and Hyman, 2008; Fu et al., 2010; Lin et al., 2010; Booth et al., 2011). The TACC3–clathrin complex has been shown to be required for kinetochore–MT integrity and the presence of a mesh of inter-MT connections within kinetochore–MT bundles (Booth et al., 2011; Hood et al., 2013; Nixon et al., 2015). This mesh has been proposed to also include GTSE1 and to serve to physically stabilize MTs within these bundles (Nixon et al., 2015). Our results suggest that Aurora A–dependent recruitment of the TACC3–clathrin complex also facilitates MT stability by recruiting GTSE1 to inhibit MCAK.

Although hyperstabilization of kinetochore–MT dynamics has been shown to influence CIN in cancer cells, the genetic and molecular defects that contribute to MT hyperstabilization and CIN in tumors remain unclear. Sequencing of cancer genomes has revealed that mutations in genes directly controlling chromosome segregation and mitosis are relatively rare (Orr and Compton, 2013). Rather, it appears that CIN may originate from changes in protein expression or activity caused by perturbed oncogenic signaling pathways (Duijf and Benezra, 2013; Orr and Compton, 2013). We show here that changing GTSE1 expression levels influences chromosome segregation and CIN. Deregulation of GTSE1 expression levels could therefore represent a molecular defect contributing to the stabilization of MT dynamics and induction of CIN in tumors through downregulation of MCAK activity. Induction of CIN in tumor cells is likely the result of complex changes in oncogenic pathways and coordinated gene expression, however, necessitating care in relating single gene perturbations in model systems to the tumor condition (Thiru et al., 2014). Our work also predicts that GTSE1 could be a CIN-related effector of increased Aurora A activity. Aurora A and its activator, TPX2, are commonly found overexpressed in tumors highly associated with CIN (Carter et al., 2006) and have been proposed to comprise an oncogenic holoenzyme (Asteriti et al., 2010). Overexpression of Aurora A has recently been shown to induce kinetochore–MT hyperstability and CIN in colorectal cancer cells, and these effects were attributed to increased MT polymerization rates (Ertych et al., 2014). Because GTSE1 spindle recruitment is dependent on Aurora A activity, it is possible that overexpression of Aurora A also results in the enhanced recruitment of GTSE1 to the spindle and increased inhibition of MCAK, which in turn could alter MT dynamics and stabilize kinetochore MTs, promoting CIN.

We have described here a novel role of GTSE1 in regulating chromosome stability through MT stability. Inhibition of MCAK activity by GTSE1 provides a new mechanism by which cells tune MT dynamics to ensure the precise balance of MT stability required for chromosome alignment and segregation.

Materials and methods

Cloning and plasmids

The hGTSE1-GFP-T2A-BSD plasmid was generated by in-frame cloning of *GTSE1* cDNA, EGFP, and T2A-BSD in an EGFP-N2 vector (Takara Bio Inc.). The GST-hGTSE1 construct used for protein purification from insect cells was generated by cloning *GTSE1* cDNA using EcoRI and BamHI restriction sites into pFLMultiBac vector modified by adding GST (Van Stedum and King, 2002; Fitzgerald et al., 2006). The GST-hGTSE1 fragment expression constructs were generated by subcloning the sequences encoding amino acids 1–460 (N terminus) and 463–739 (C terminus) in a pGEX-6p-1rbs vector (GE Healthcare) using BamHI and SalI restriction sites. An N-terminal FLAG-LAP NFLAP cassette was recombined onto the N terminus of *GTSE1* encoded on the BAC RP11-1152E11 via Red E/T–based recombination (Zhang et al., 1998; Poser et al., 2008). An mCherry-BSD cassette was recombined onto the C terminus of mH2A.Z encoded on the BAC RP24-363J17 via Red E/T–based recombination (Zhang et al., 1998; Poser et al., 2008).

Cell culture and cell lines

All cell lines were grown in DMEM (PAN Biotech) containing 10% FBS (Gibco), 2 mM L-glutamine (PAN Biotech), 100 U/ml penicillin, and 0.1 mg/ml streptomycin (PAN Biotech) at 37°C in 5% CO_2. U2OS cells stably expressing RNAi-resistant wild-type and SxIP-mutated GTSE1-LAP were described previously (Scolz et al., 2012). HCT116 $p53^{-/-}$ and U2OS-PA-GFP-tubulin cells were gifts from D. Compton (Dartmouth Medical School, Hanover, NH). U2OS cells expressing NFLAP-GTSE1, GTSE1-$LAP^{WT(303)}$, and mH2A.Z-mCherry were generated by transfecting the respective BACs using Effectene according to the manufacturer's protocol and selecting for stable transfectants. HeLa cells expressing BAC-based hKif2C-LAP were a gift from A. Hyman (Max Planck Institute of Molecular Cell Biology and Genetics, Dresden, Germany). HCT116 and HCT116 $p53^{-/-}$ cells grown in 6-cm dishes were transfected with 1.5 µg hGTSE1-GFP-T2A-BSD cDNA using 5 µl Lipofectamine 2000 (Invitrogen) according to the manufacturer's protocol. Stable line populations were selected on 4 µg/ml BSD, and individual clones were isolated. HCT116 and HCT116 $p53^{-/-}$ control clones were isolated after treating the cells with Lipofectamine 2000 in the absence of DNA.

Generation of *GTSE1* knockouts using the CRISPR-Cas9 system

To generate *GTSE1* knockout cells using the CRISPR-Cas9 system, two different target sites were chosen in *GTSE1* downstream of the ATG in exon 2 (5′-GGCAGGCTGAAGGCTCATCG-3′) and exon 9 (5′-AAG GCCAGAGCAGCGCCGGC-3′). Plasmids expressing the Cas9 nuclease and the corresponding guide RNAs were obtained by cloning the primer pairs 5′-CACCGAAGGCCAGAGCAGCGCCGGC-3′ and 5′-AAACGCCGGCGCTGCTCTGGCCTTC-3′ and 5′-CACCGGCAG GCTGAAGGCTCATCG-3′ and 5′-AAACCGATGAGCCTTCAG CCTGCC-3′ into the pX330 background (Addgene) as described by Ran et al. (2013). U2OS cells were transfected with individual plasmids targeting a single site or with two plasmids targeting both sites simultaneously, and clones were isolated by serial dilution 48 h after transfection. Genomic DNA was prepared using the DNeasy Blood and Tissue kit (QIAGEN). The regions surrounding the CRISPR-Cas9 sites were amplified using the primers 5′-CGGCAATGAGTCTCCCTC AG-3′ and 5′-AATCGCTTGAACCCGAAAGG-3′ (for the site in exon

2) or 5′-CAGTCCACAGCAAATGCCAG-3′ and 5′-CACGACTGA GGTGTGACTTC-3′ (for the site in exon 9), and the corresponding PCR products were sequenced using primers 5′-CCCTGGGATGCG ATCATTTC-3′ or 5′-CCCTCAGCACTGCATTAGCAC-3′, respectively. Heterozygous insertions and deletions were resolved using the TIDE software (Netherlands Cancer Institute; Brinkman et al., 2014). TIDE compares sequence traces (from capillary sequencing runs) between a reference run (wild-type sequence) and a sample run (modified sequence) to identify mutations, insertions, and deletions in the sample sequence. It also calculates the proportion of modifications at a given site in the modified DNA.

Generation of GFP knock-in at endogenous GTSE1 via CRISPR-Cas9

To generate the U2OS GTSE1-GFP knock-in, a BAC containing a GTSE1-GFP-T2A-BSD^R, fusion was first generated via Red E/T–based recombination of a GFP-T2A-BSD^R cassette (gift from A. Hyman, Max Planck Institute of Molecular Cell Biology and Genetics, Dresden, Germany) amplified with the primers 5′-TGAGCCCTGAGGCTG ACAAGGAGAACGTGGATTCCCCACTCCTCAAGTTCGAGAATC TTTATTTTCAGGGCG-3′ and 5′-CAAGTGTAAGCCACTGCGACC AGCCTAAAGCTTGTTT CTGAGGGTTGAAAATTAACCCTCC CACACGTAGCC-3′ into a BAC containing GTSE1. The template for Cas9-mediated homologous recombination was obtained by amplifying from the GTSE1-GFP-T2A-BSD^R BAC a region encompassing the GFP-T2A-BSD^R cassette and 1-kbp homology arms to the C terminus of GTSE1 using primers 5′-CATCAGCCAAGTGAACGAGC-3′ and 5′-GAATCACGCAGTAACCGCAG-3′. The plasmid expressing the Cas9 nuclease and the guide RNA targeting the C terminus of GTSE1 was obtained by cloning the primer pair 5′-CACCGTTGAAAGAAC AGCCCTAAAG-3′ and 5′-AAACCTTTAGGGCTGTTCTTTCAAC-3′ into the pX330 background.

RNAi

siRNA against hGTSE1 (5′-GAUUCAUACAGGAGUCAAA-3′), MCAK (5′-GAUCCAACGCAGUAAUGGU-3′), and control siRNA (Silencer negative control 2; AM4637) were purchased from Ambion. siRNA against hKif2A (2, 5′-CUACACAACUUGAAGCUAU-3′; and 4, 5′-GACCCUCCUUCAAGAGAUA-3′) were purchased from Sigma-Aldrich. Approximately 35,000 U2OS cells were added to prewarmed media in 24-well plates or 8-well imaging chambers (ibidi), and transfection complexes containing 2.5 µl Oligofectamine and siRNA were added immediately afterward. Media was changed after 6–8 h. Final concentrations of 80 nM and 12 nM RNAi were used for GTSE1 and MCAK, respectively. For Kif2A, a final concentration of 100 nM was used by mixing siRNAs 2 and 4. All experiments were performed 48 h after siRNA transfection.

Antibodies

Rabbit antibodies against hGTSE1 were previously described (Scolz et al., 2012). Goat anti-GFP antibodies used in immunoprecipitation assays were previously described (Poser et al., 2008). Rabbit antibody against CEP135 was previously described (Bird and Hyman, 2008). Mouse monoclonal antibody conjugated with Alexa Fluor 488 against Mad1 was a gift from A. Musacchio (Max Planck Institute of Molecular Physiology, Dortmund, Germany). Rabbit anti-pTACC3 was a gift from K. Kinoshita (Institute of Physical and Chemical Research, Wako, Japan). The following antibodies were obtained from commercial sources: mouse anti–α-tubulin (DM1α; Sigma-Aldrich), mouse anti-MCAK (clone 1G2; Abnova), human nuclear antibodies to nuclear antigens–centromere autoantibody (CREST; CS1058; Europa Bioproducts Ltd.), mouse anti–c-myc (Oncogene/EMD Millipore), rat anti-EB1 (clone KT-51; Absea Biotechnology), rabbit anti-TACC3 (H-300; Santa Cruz Biotechnology, Inc.), rabbit anti–ch-TOG (86073; Abcam), rabbit anti–Aurora B (2254; Abcam), rabbit anti-Kif2A (NB500-180; Novus Biologicals), and rabbit anti-GFP (AB6556; Abcam). The following secondary antibodies were used: donkey anti–mouse, anti–rabbit, or anti–rat antibodies conjugated to Alexa Fluor 488, 594, or 647 (Bethyl Laboratories, Inc.) and donkey anti–human antibody conjugated to Texas red or Cy5 (Jackson ImmunoResearch Laboratories, Inc.).

Immunofluorescence

Cells on coverslips were fixed using −20°C methanol for 10 min. Cells were blocked with 0.2% fish skin gelatin (Sigma-Aldrich) in PBS. Cells were incubated with primary antibodies in 0.2% fish skin gelatin in PBS for 1 h at 37°C in a humidified chamber and washed, and the same was repeated with secondary antibodies. Coverslips were mounted with ProLong gold with DAPI (Molecular Probes and Thermo Fisher Scientific). Quantification of TACC3 on the inner spindle of U2OS cells after control and GTSE1 RNAi and in GTSE1 knockout clones was performed after fixation in 4% PFA dissolved in Pipes (50 mM Pipes, pH 7.2, 10 mM EGTA, 1 mM $MgCl_2$, and 0.2% Triton X-100).

Microscopy and live-cell imaging

FDAPA analysis and images used for quantifying astral length, inner spindle intensity, spindle orientation, and TACC3 and MCAK spindle localization were acquired using a Marianas (Intelligent Imaging Innovations) spinning-disk confocal system based on a microscope (Axio Observer Z1; ZEISS) equipped with a camera (ORCA-Flash 4.0; Hamamatsu Photonics). Images were taken using a 63× 1.4 NA Apochromat objective (ZEISS). Images for TACC spindle localization in U2OS cells were taken using a 100× 1.4 NA Plan-Apochromat objective (ZEISS). The images were z-projected using Slidebook software 5.5 (Intelligent Imaging Innovations). All other images were acquired using a DeltaVision imaging system (GE Healthcare) equipped with an sCMOS camera (PCO Edge 5.5). Images were taken using a 60× 1.42 NA PlanApo-N objective (Olympus) at room temperature. Serial z stacks of 0.2-µm thickness were obtained and deconvolved using SoftWoRx software 6.1.l. For live-cell imaging, media was changed to CO_2-independent media (Gibco) 12 h before imaging. Live-cell image sequences were acquired at 1-min intervals for 12 h in 2-µm serial z sections using a 40× 1.42 NA UPlanFL-N objective (Olympus) at 37°C.

Image quantification and data analysis

Inner spindle intensity and TACC3 and MCAK spindle localization were quantified in three dimensions using the surface module in IMARIS software (Bitplane). Astral MT lengths were measured in three dimensions using IMARIS software. Astral MT length measurements using EB1 comets were performed as described by Stout et al. (2011). In brief, the position of every EB1 comet was determined using the point function of the IMARIS software, and the angle it formed with the spindle axis was calculated. Each comet with an angle superior to the one formed by the spindle axis and the outermost spindle MT was considered an astral comet, and its distance to the closest pole was calculated. Total numbers of EB1 astral MT comets were quantified using IMARIS software. To measure spindle tilt, both spindle poles were located in the z series and then, using the angle tool in Slidebook software 5.5, the angle made by the spindle to the substratum was measured. Images were processed with ImageJ (National Institutes of Health) or Photoshop (Adobe).

Determining kinetochore–MT half-life by FDAPA

FDAPA in U2OS cells expressing PA-GFP-tubulin was performed as described by Bakhoum et al. (2009b). U2OS-PA-GFP-tubulin cells grown on a poly-L-lysine (Sigma-Aldrich)–coated 3.5-cm glass-bottom

chamber (ibidi) were treated with either control or GTSE1 RNAi for 48 h. The medium was changed to CO_2-independent media 12 h before the experiment. PA-GFP-tubulin in a small area around the kinetochore–MT attachment region on one half of the metaphase spindle was activated with a 405-nm laser, and images were taken every 10 s for 5 min. Fluorescence intensity after activation was measured at each time point using ImageJ. Fluorescence intensity, measured within a similar region on the other (nonactivated) half spindle, was used for background subtraction. Values were corrected for photobleaching by normalizing to values obtained from taxol-treated stabilized spindles. After background subtraction and correction for photobleaching, values were normalized to the first time point and were fitted to the double exponential decay curve $F = A1 \times \exp(-k1 \times t) + A2 \times \exp(-k2 \times t)$ using Prism (GraphPad Software), where $A1$ and $A2$ are the percentages of the total fluorescence contribution of the nonkinetochore and kinetochore MTs, $k1$ and $k2$ are their respective decay rate constants, and t is the time after photoactivation. The half-life of kinetochore MTs was calculated using $T1/2 = \ln 2/k_2$.

Kinetochore–MT stability assays and determining Mad1-positive kinetochores

U2OS cells treated with either control or GTSE1 RNAi were arrested using Cdk1 inhibitor (RO-3306; EMD Millipore) at 31 h after RNAi transfection. Cells were arrested for 17 h and then released in normal media for 1 h. After 1 h of release, the cells were immediately transferred to ice-cold media for 17 min and fixed in −20°C methanol. To determine the ratio of Mad1-positive kinetochores, U2OS cells treated with either control or GTSE1 RNAi were arrested using the Cdk1 inhibitor as mentioned for the kinetochore–MT stability assay. After 1 h of release, the cells were fixed with 4% PFA and permeabilized with 0.1% Triton X-100. The ratio of Mad1-positive kinetochores was determined by quantifying the total number of kinetochores in aligned metaphase plates and then quantifying the number of Mad1-positive kinetochores using the Coloc tool in IMARIS software.

K-fiber localization of GTSE1

U2OS cells expressing BAC-based GTSE1-LAP$^{WT(303)}$ were arrested using Cdk1 inhibitor for 17 h and then released in normal media for 1 h. After 1 h of release, the cells were immediately transferred to ice-cold media for 17 min and fixed using 4% PFA dissolved in Pipes (50 mM Pipes, pH 7.2, 10 mM EGTA, 1 mM $MgCl_2$, and 0.2% Triton X-100). GTSE1 localization to kinetochore fibers was studied using a Marianas spinning-disk confocal system based on a microscope (Axio Observer Z1). Images were taken using a 100× 1.4 NA Plan-Apochromat objective.

Immunoprecipitation

Cells with ∼70% confluency were arrested in mitosis by adding 200 ng/ml nocodazole for 18 h. Mitotic cells were harvested by shakeoff and lysed using cell lysis buffer (50 mM Hepes, pH 7.2, 50 mM Na_2HPO_4, 150 mM NaCl, 10% glycerol, 1% Triton X-100, 1 mM EGTA, 1.5 mM $MgCl_2$, and protease inhibitors) followed by centrifugation at 13,000 rpm for 10 min at 4°C to clear the lysate. A part of the supernatant was taken as input, and 1–2 µg of the indicated antibody was added to the remaining supernatant and incubated for 2 h at 4°C with rotation. Dynabeads coupled to protein G (Novex Life Technology) were added to the extracts and incubated for 4 h at 4°C. The beads were washed three times with cell lysis buffer and once with 1× PBS. The beads were resuspended in hot Lamelli buffer and analyzed by Western blotting.

Western blots

For Western blotting after RNAi, cells were harvested by directly adding hot Lamelli buffer in 24-well plates. The proteins were separated on SDS-PAGE gels and transferred onto nitrocellulose membranes. The membrane was incubated with the indicted primary antibodies. The secondary antibodies were coupled to horseradish peroxidase and protein bands and were detected using enhanced chemiluminescence (GE Healthcare).

Protein purification

A full-length human *GTSE1* cDNA sequence was cloned into pFL-MultiBac vectors, and baculovirus-generated hGTSE1-FL protein was expressed in Tnao38 insect cells at 27°C for 48 h. The cells were harvested by centrifugation at 1,800 rpm for 15 min in a Sorvall RC 3BP Plus centrifuge (Thermo Fisher Scientific). The cell pellet was either stored at −80°C or processed immediately. The cell pellet from 1-liter culture was resuspended in 100 ml ice-cold buffer A (50 mM Hepes, pH 8.0, 300 mM NaCl, 5% glycerol, 2 mM Tris(2-carboxyethyl)phosphine, and protease inhibitors [Serva]) lysed by sonication and clarified by centrifuging at 29,000 rpm for 50 min at 4°C. The cell lysate was incubated with 1 ml glutathione resin (Amintra) for 1 h at 4°C. The resin beads were loaded on gravity flow columns and washed with 150 ml buffer A at 4°C. hGTSE1 was cleaved from the beads using GST Precision (Max Planck Institute of Molecular Physiology) overnight at 4°C. The protein was eluted and concentrated using Amicon concentrators. The protein was further purified by size exclusion in a Superdex 200 10/300 column (GE Healthcare) using gel filtration buffer (30 mM Hepes, pH 8, 300 mM NaCl, 5% glycerol, and 2 mM Tris(2-carboxyethyl)phosphine). The peak fractions were collected and concentrated in Amicon concentrators to give a final concentration of 5–10 µM. The hGTSE1 1–460 and 463–739 fragments and GST were cloned into pGEX-6p-1rbs vector and expressed in bacteria. Bacteria were grown to OD 600 of 0.8 and were induced using 1 mM IPTG at 20°C overnight. The bacterial cells were pelleted at 4,000 rpm for 20 min at room temperature. Cells were resuspended in GST binding buffer (25 mM Hepes, pH 7.5, 300 mM NaCl, 1 mM EDTA, 5% glycerol, 1% Triton X-100, and DNase), lysed by sonication, and cleared by centrifugation at 29,000 rpm for 30 min at 4°C. The cleared lysate was incubated with glutathione resin (Amintra) overnight at 4°C. The beads were washed with GST binding buffer, and the protein was used for experiments. MCAK-His6 was expressed in Sf9 cells and purified by a sequence of cation exchange, nickel affinity, and size-exclusion chromatography (Helenius et al., 2006).

Pulldowns

In vitro GST pulldowns were performed in GST binding buffer by incubating equal amounts of purified full-length MCAK with GST alone or with GST-hGTSE1 1–460 and 463–739 fragments (immobilized on glutathione resin) for 1 h at 4°C. The reactions were washed with GST binding buffer, resuspended in hot Lamelli buffer, and analyzed by Western blotting.

MT pelleting assays

Taxol-stabilized MTs were prepared by incubating MTs with 1 mM GTP at 37°C for 30 min, followed by incubation at 37°C for 5 min after the addition of 50 µM taxol. 1.66 µM tubulin was added to a reaction mixture of 200 nM MCAK and increasing amounts of GTSE1. All reactions were performed in BRB80 buffer (80 mM Pipes, pH 6.8, 1 mM EGTA, and 1 mM $MgCl_2$) and supplemented with 70 mM KCl, 1.5 mM ATP, and 10 µM taxol for 1 h at room temperature. The reaction was then layered onto a cushion buffer (80 mM Pipes, 1 mM EGTA, 1 mM $MgCl_2$, and 50% glycerol) in a microcentrifuge tube and was centrifuged at 90,000 rpm in a TLA-120.1 rotor (Beckman Coulter) for 10 min at 25°C. Supernatant and pellet fractions were separated by SDS-PAGE and stained with Coomassie blue for analysis.

TIRF microscopy assays for MT dynamics and MCAK activity

For tubulin and MT preparation, tubulin was purified from juvenile bovine brains using a modified version of the high-Pipes method (Castoldi and Popov, 2003), wherein the first polymerization cycle was performed in 100 mM Pipes instead of 1 M Pipes. Tetramethylerhodamine (TAMRA) and Alexa Fluor 546 succinimidyl esters were used to label ε-amines on tubulin (Hyman et al., 1991). The labeling reaction was performed on polymerized tubulin so as not to modify the polymerization interfaces. GMPCPP-stabilized MTs were prepared as follows: a polymerization mixture was prepared with BRB80 (80 mM Pipes-KOH, pH 6.9, 1 mM EGTA, and 1 mM $MgCl_2$) and 2 mM tubulin, 1 mM GMPCPP (Jena Biosciences), 1 mM $MgCl_2$, and a 1:4 molar ratio of TAMRA-labeled/unlabeled tubulin. The mixture was incubated on ice for 5 min followed by incubation at 37°C for 2 h. The polymerized GMPCPP MTs were centrifuged at maximum speed in an Airfuge (Beckman Coulter) and resuspended in BRB80. GMPCPP seeds were prepared by polymerizing a 1:4 molar ratio of TAMRA-labeled/unlabeled tubulin in the presence of GMPCPP in two cycles as described previously (Gell et al., 2010). GMPCPP seeds prepared in this way were stable for several months at −80°C.

For TIRF microscopy and preparation of microscope chambers, the microscope setup used a microscope chassis (Axiovert Z1; ZEISS), a 100× 1.45 NA Plan-Apochromat objective lens, and the TIRF III slider (ZEISS). A λ = 491-nm diode-pumped solid-state laser (Cobolt) was coupled to a fiber optic cable in free space and introduced into the slider. Epifluorescence was achieved using a PhotofluorII excitation source (89 North) with wavelength-specific filter cubes (Chroma Technology Corp.). Images were recorded using an iXon with DV-897 electron-multiplying charge-coupled device cameras (Andor Technology). Microscope chambers were constructed using custom-machined mounts (Gell et al., 2010). In brief, cover glass was cleaned and silanized as described previously (Helenius et al., 2006). Cover glasses (22 × 22 mm and 18 × 18 mm) were separated by two layers of double-sided tape, creating a channel for the exchange of solution. Image acquisition was controlled using MetaMorph (Molecular Devices).

Seeds or GMPCPP-stabilized MTs, depending on the experiment, were adhered to silanized glass slides as described previously (Bechstedt and Brouhard, 2012). On the day of each experiment for the dynamic assay, aliquots of unlabeled and Alexa Fluor 546–labeled tubulin were thawed, mixed to a 1:3 molar labeling ratio, aliquoted again, and stored in liquid nitrogen.

MT growth from GMPCPP seeds was achieved by incubating flow channels with tubulin in standard polymerization buffer, comprised of BRB80, 1 mM GTP, 0.1 mg/ml BSA, 1% 2-mercaptoethanol, 250 nM glucose oxidase, 64 nM catalase, and 40 mM D-glucose. Assays were performed with an objective heater set to 35°C. Time-lapse image sequences were acquired at 5-s intervals. MCAK depolymerization of GMPCPP-stabilized seeds was achieved by incubating flow channels with MCAK and standard polymerization buffer plus ATP (BRB80, 1 mM GTP, 0.1 mg/ml BSA, 1% 2-mercaptoethanol, 250 nM glucose oxidase, 64 nM catalase, 40 mM D-glucose, and 1 mM ATP). Assays were performed with an objective heater set to 35°C. Time-lapse image sequences were acquired at 5-s intervals.

For MT growth and shrinkage rates, MT growth rates were analyzed by manually fitting lines to kymographs of growing MTs using the Kymograph and Linescan features in MetaMorph.

FISH

HCT116 and HCT116 $p53^{-/-}$ cells grown on 22-mm coverslips were washed once with 1× PBS and fixed with 3:1 methanol–acetic acid solution at room temperature for 30 min. Cells on coverslips were dried at room temperature for 10 min and immersed in 2× SSC (0.3 M NaCl and 30 mM sodium citrate) for 5 min at room temperature. Cells were dehydrated in ethanol series (70%, 85%, and 100%), each for 5 min at room temperature, and then air dried for 10 min. Cells were processed for FISH by using specific α-satellite probes against chromosomes 7 and 11 (Cytocell) according to the manufacturer's protocol. Coverslips were mounted using ProLong gold with DAPI overnight at room temperature and sealed. Chromosome signals from ∼1,000 cells were scored using the criteria outlined in Van Stedum and King (2002).

Statistical analysis

Statistical significance was determined by performing two-tailed Student's *t* tests with unequal variance, unless otherwise stated. Statistical analysis of all karyotype studies, quantification of lagging chromosomes in *GTSE1*-overexpressing clonal cell lines, and phenotype quantification in *GTSE1* knockout clonal cell lines were performed using χ^2 tests.

Online supplemental material

Fig. S1 contains Western blots showing the RNAi depletion efficiency for all siRNAs and cell lines analyzed. Fig. S2 contains verification and characterization of Cas9 nuclease-mediated GTSE1-GFP and GTSE1 knockout clones. Fig. S3 includes analysis of kinetochore–MT stability, TACC3 localization, and Kif2A dependence after perturbation of GTSE1 expression. Fig. S4 shows purified GTSE1 and MCAK proteins used and in vitro analysis of GTSE1 inhibition of MCAK. Fig. S5 contains quantification of different categories of anaphase chromosome segregation defects in U2OS and HeLa cells after GTSE1 and/or MCAK RNAi depletion. Videos 1 and 2 show chromosome dynamics and mitotic progression in control (Video 1) and GTSE1-depleted (Video 2) U2OS cells. Videos 3 and 4 show GTSE1 localization to kinetochore MTs in z sections from a cold-treated fixed cell labeled by CREST antibody and GTSE1 (Video 3) and tubulin (Video 4). Videos 5 and 6 show MCAK activity on GMPCPP-stabilized MTs with MCAK alone (Video 5) or MCAK and GTSE1 (Video 6).

Acknowledgments

We thank D. Compton for providing the U2OS PA-GFP-tubulin and HCT116 $p53^{-/-}$ cell lines. We thank A. Musacchio and G. Vader for comments on the manuscript. We thank S. Maffini for help with performing and analyzing photoactivation experiments, A. Faesen for advice and help with MT sedimentation assays, M. Mattiuzzo for help with FISH, and J. Beermann and K. Klare for help with protein purification.

This work was supported by the Max Planck Institute of Molecular Physiology, Worldwide Cancer Research project grant 16-0093 to A.W. Bird, and an International Max Planck Research School in Chemical and Molecular Biology PhD fellowship to S. Bendre.

The authors declare no competing financial interests.

Author contributions: S. Bendre, C. Hall, A. Rondelet, G.J. Brouhard, and A.W. Bird conceived and designed experiments. S. Bendre and A. Rondelet performed all cellular assays, image quantification, and analysis. S. Bendre performed all protein interaction studies and GTSE1 purification. C. Hall performed TIRF imaging experiments and analysis. A. Rondelet designed, created, verified, and characterized CRISPR-Cas9 knockout cell lines. N. Schmidt created CRISPR-Cas9 knockout cell lines. Y.-C. Lin created GST fusion constructs. S. Bendre and A.W. Bird wrote the manuscript.

Submitted: 17 June 2016
Revised: 4 October 2016
Accepted: 21 October 2016

References

Andrews, P.D., Y. Ovechkina, N. Morrice, M. Wagenbach, K. Duncan, L. Wordeman, and J.R. Swedlow. 2004. Aurora B regulates MCAK at the mitotic centromere. *Dev. Cell.* 6:253–268. http://dx.doi.org/10.1016/S1534-5807(04)00025-5

Asteriti, I.A., W.M. Rensen, C. Lindon, P. Lavia, and G. Guarguaglini. 2010. The Aurora-A/TPX2 complex: a novel oncogenic holoenzyme? *Biochim. Biophys. Acta.* 1806:230–239.

Bakhoum, S.F., G. Genovese, and D.A. Compton. 2009a. Deviant kinetochore microtubule dynamics underlie chromosomal instability. *Curr. Biol.* 19:1937–1942. http://dx.doi.org/10.1016/j.cub.2009.09.055

Bakhoum, S.F., S.L. Thompson, A.L. Manning, and D.A. Compton. 2009b. Genome stability is ensured by temporal control of kinetochore-microtubule dynamics. *Nat. Cell Biol.* 11:27–35. http://dx.doi.org/10.1038/ncb1809

Bakhoum, S.F., W.T. Silkworth, I.K. Nardi, J.M. Nicholson, D.A. Compton, and D. Cimini. 2014. The mitotic origin of chromosomal instability. *Curr. Biol.* 24:R148–R149. http://dx.doi.org/10.1016/j.cub.2014.01.019

Bechstedt, S., and G.J. Brouhard. 2012. Doublecortin recognizes the 13-protofilament microtubule cooperatively and tracks microtubule ends. *Dev. Cell.* 23:181–192. http://dx.doi.org/10.1016/j.devcel.2012.05.006

Bird, A.W., and A.A. Hyman. 2008. Building a spindle of the correct length in human cells requires the interaction between TPX2 and Aurora A. *J. Cell Biol.* 182:289–300. http://dx.doi.org/10.1083/jcb.200802005

Bird, A.W., A. Erler, J. Fu, J.-K. Hériché, M. Maresca, Y. Zhang, A.A. Hyman, and A.F. Stewart. 2011. High-efficiency counterselection recombineering for site-directed mutagenesis in bacterial artificial chromosomes. *Nat. Methods.* 9:103–109. http://dx.doi.org/10.1038/nmeth.1803

Booth, D.G., F.E. Hood, I.A. Prior, and S.J. Royle. 2011. A TACC3/ch-TOG/clathrin complex stabilises kinetochore fibres by inter-microtubule bridging. *EMBO J.* 30:906–919. http://dx.doi.org/10.1038/emboj.2011.15

Braun, A., K. Dang, F. Buslig, M.A. Baird, M.W. Davidson, C.M. Waterman, and K.A. Myers. 2014. Rac1 and Aurora A regulate MCAK to polarize microtubule growth in migrating endothelial cells. *J. Cell Biol.* 206:97–112. http://dx.doi.org/10.1083/jcb.201401063

Brinkman, E.K., T. Chen, M. Amendola, and B. van Steensel. 2014. Easy quantitative assessment of genome editing by sequence trace decomposition. *Nucleic Acids Res.* 42. http://dx.doi.org/10.1093/nar/gku936

Burns, K.M., M. Wagenbach, L. Wordeman, and D.C. Schriemer. 2014. Nucleotide exchange in dimeric MCAK induces longitudinal and lateral stress at microtubule ends to support depolymerization. *Structure.* 22:1173–1183. http://dx.doi.org/10.1016/j.str.2014.06.010

Carter, S.L., A.C. Eklund, I.S. Kohane, L.N. Harris, and Z. Szallasi. 2006. A signature of chromosomal instability inferred from gene expression profiles predicts clinical outcome in multiple human cancers. *Nat. Genet.* 38:1043–1048. http://dx.doi.org/10.1038/ng1861

Castoldi, M., and A.V. Popov. 2003. Purification of brain tubulin through two cycles of polymerization-depolymerization in a high-molarity buffer. *Protein Expr. Purif.* 32:83–88. http://dx.doi.org/10.1016/S1046-5928(03)00218-3

Cheeseman, L.P., E.F. Harry, A.D. McAinsh, I.A. Prior, and S.J. Royle. 2013. Specific removal of TACC3-ch-TOG-clathrin at metaphase deregulates kinetochore fiber tension. *J. Cell Sci.* 126:2102–2113. http://dx.doi.org/10.1242/jcs.124834

Cong, L., F.A. Ran, D. Cox, S. Lin, R. Barretto, N. Habib, P.D. Hsu, X. Wu, W. Jiang, L.A. Marraffini, and F. Zhang. 2013. Multiplex genome engineering using CRISPR/Cas systems. *Science.* 339:819–823. http://dx.doi.org/10.1126/science.1231143

Cooper, J.R., M. Wagenbach, C.L. Asbury, and L. Wordeman. 2009. Catalysis of the microtubule on-rate is the major parameter regulating the depolymerase activity of MCAK. *Nat. Struct. Mol. Biol.* 17:77–82. http://dx.doi.org/10.1038/nsmb.1728

Cross, M.K., and M.A. Powers. 2011. Nup98 regulates bipolar spindle assembly through association with microtubules and opposition of MCAK. *Mol. Biol. Cell.* 22:661–672. http://dx.doi.org/10.1091/mbc.E10-06-0478

Desai, A., S. Verma, T.J. Mitchison, and C.E. Walczak. 1999. Kin I kinesins are microtubule-destabilizing enzymes. *Cell.* 96:69–78. http://dx.doi.org/10.1016/S0092-8674(00)80960-5

Domnitz, S.B., M. Wagenbach, J. Decarreau, and L. Wordeman. 2012. MCAK activity at microtubule tips regulates spindle microtubule length to promote robust kinetochore attachment. *J. Cell Biol.* 197:231–237. http://dx.doi.org/10.1083/jcb.201108147

Duijf, P.H.G., and R. Benezra. 2013. The cancer biology of whole-chromosome instability. *Oncogene.* 32:4727–4736. http://dx.doi.org/10.1038/onc.2012.616

Ems-McClung, S.C., S.G. Hainline, J. Devare, H. Zong, S. Cai, S.K. Carnes, S.L. Shaw, and C.E. Walczak. 2013. Aurora B inhibits MCAK activity through a phosphoconformational switch that reduces microtubule association. *Curr. Biol.* 23:2491–2499. http://dx.doi.org/10.1016/j.cub.2013.10.054

Ertych, N., A. Stolz, A. Stenzinger, W. Weichert, S. Kaulfuß, P. Burfeind, A. Aigner, L. Wordeman, and H. Bastians. 2014. Increased microtubule assembly rates influence chromosomal instability in colorectal cancer cells. *Nat. Cell Biol.* 16:779–791. http://dx.doi.org/10.1038/ncb2994

Fitzgerald, D.J., P. Berger, C. Schaffitzel, K. Yamada, T.J. Richmond, and I. Berger. 2006. Protein complex expression by using multigene baculoviral vectors. *Nat. Methods.* 3:1021–1032. http://dx.doi.org/10.1038/nmeth983

Fu, W., W. Tao, P. Zheng, J. Fu, M. Bian, Q. Jiang, P.R. Clarke, and C. Zhang. 2010. Clathrin recruits phosphorylated TACC3 to spindle poles for bipolar spindle assembly and chromosome alignment. *J. Cell Sci.* 123:3645–3651. http://dx.doi.org/10.1242/jcs.075911

Gell, C., V. Bormuth, G.J. Brouhard, D.N. Cohen, S. Diez, C.T. Friel, J. Helenius, B. Nitzsche, H. Petzold, J. Ribbe, et al. 2010. Microtubule dynamics reconstituted in vitro and imaged by single-molecule fluorescence microscopy. *Methods Cell Biol.* 95:221–245. http://dx.doi.org/10.1016/S0091-679X(10)95013-9

Giet, R., D. McLean, S. Descamps, M.J. Lee, J.W. Raff, C. Prigent, and D.M. Glover. 2002. *Drosophila* Aurora A kinase is required to localize D-TACC to centrosomes and to regulate astral microtubules. *J. Cell Biol.* 156:437–451. http://dx.doi.org/10.1083/jcb.200108135

Gordon, D.J., B. Resio, and D. Pellman. 2012. Causes and consequences of aneuploidy in cancer. *Nat. Rev. Genet.* 13:189–203.

Helenius, J., G. Brouhard, Y. Kalaidzidis, S. Diez, and J. Howard. 2006. The depolymerizing kinesin MCAK uses lattice diffusion to rapidly target microtubule ends. *Nature.* 441:115–119. http://dx.doi.org/10.1038/nature04736

Hood, F.E., S.J. Williams, S.G. Burgess, M.W. Richards, D. Roth, A. Straube, M. Pfuhl, R. Bayliss, and S.J. Royle. 2013. Coordination of adjacent domains mediates TACC3-ch-TOG-clathrin assembly and mitotic spindle binding. *J. Cell Biol.* 202:463–478. http://dx.doi.org/10.1083/jcb.201211127

Howell, B.J., B. Moree, E.M. Farrar, S. Stewart, G. Fang, and E.D. Salmon. 2004. Spindle checkpoint protein dynamics at kinetochores in living cells. *Curr. Biol.* 14:953–964. http://dx.doi.org/10.1016/j.cub.2004.05.053

Hubner, N.C., A.W. Bird, J. Cox, B. Splettstoesser, P. Bandilla, I. Poser, A. Hyman, and M. Mann. 2010. Quantitative proteomics combined with BAC TransgeneOmics reveals in vivo protein interactions. *J. Cell Biol.* 189:739–754. http://dx.doi.org/10.1083/jcb.200911091

Hunter, A.W., M. Caplow, D.L. Coy, W.O. Hancock, S. Diez, L. Wordeman, and J. Howard. 2003. The kinesin-related protein MCAK is a microtubule depolymerase that forms an ATP-hydrolyzing complex at microtubule ends. *Mol. Cell.* 11:445–457. http://dx.doi.org/10.1016/S1097-2765(03)00049-2

Hyman, A., D. Drechsel, D. Kellogg, S. Salser, K. Sawin, P. Steffen, L. Wordeman, and T. Mitchison. 1991. Preparation of modified tubulins. *Methods Enzymol.* 196:478–485. http://dx.doi.org/10.1016/0076-6879(91)96041-O

Jiang, K., J. Wang, J. Liu, T. Ward, L. Wordeman, A. Davidson, F. Wang, and X. Yao. 2009. TIP150 interacts with and targets MCAK at the microtubule plus ends. *EMBO Rep.* 10:857–865. http://dx.doi.org/10.1038/embor.2009.94

Kinoshita, K., T.L. Noetzel, L. Pelletier, K. Mechtler, D.N. Drechsel, A. Schwager, M. Lee, J.W. Raff, and A.A. Hyman. 2005. Aurora A phosphorylation of TACC3/maskin is required for centrosome-dependent microtubule assembly in mitosis. *J. Cell Biol.* 170:1047–1055. http://dx.doi.org/10.1083/jcb.200503023

Kline-Smith, S.L., A. Khodjakov, P. Hergert, and C.E. Walczak. 2003. Depletion of centromeric MCAK leads to chromosome congression and segregation defects due to improper kinetochore attachments. *Mol. Biol. Cell.* 15:1146–1159. http://dx.doi.org/10.1091/mbc.E03-08-0581

Lan, W., X. Zhang, S.L. Kline-Smith, S.E. Rosasco, G.A. Barrett-Wilt, J. Shabanowitz, D.F. Hunt, C.E. Walczak, and P.T. Stukenberg. 2004. Aurora B phosphorylates centromeric MCAK and regulates its

localization and microtubule depolymerization activity. *Curr. Biol.* 14:273–286. http://dx.doi.org/10.1016/j.cub.2004.01.055

Li, C., Y. Zhang, Q. Yang, F. Ye, S.Y. Sun, E.S. Chen, and Y.-C. Liou. 2016. NuSAP modulates the dynamics of kinetochore microtubules by attenuating MCAK depolymerisation activity. *Sci. Rep.* 6. http://dx.doi.org/10.1038/srep18773

Lin, C.-H., C.-K. Hu, and H.-M. Shih. 2010. Clathrin heavy chain mediates TACC3 targeting to mitotic spindles to ensure spindle stability. *J. Cell Biol.* 189:1097–1105. http://dx.doi.org/10.1083/jcb.200911120

Maney, T., A.W. Hunter, M. Wagenbach, and L. Wordeman. 1998. Mitotic centromere-associated kinesin is important for anaphase chromosome segregation. *J. Cell Biol.* 142:787–801. http://dx.doi.org/10.1083/jcb.142.3.787

Marumoto, T., S. Honda, T. Hara, M. Nitta, T. Hirota, E. Kohmura, and H. Saya. 2003. Aurora-A kinase maintains the fidelity of early and late mitotic events in HeLa cells. *J. Biol. Chem.* 278:51786–51795. http://dx.doi.org/10.1074/jbc.M306275200

Meunier, S., and I. Vernos. 2011. K-fibre minus ends are stabilized by a RanGTP-dependent mechanism essential for functional spindle assembly. *Nat. Cell Biol.* 13:1406–1414. http://dx.doi.org/10.1038/ncb2372

Monte, M., L. Collavin, D. Lazarević, R. Utrera, T.A. Dragani, and C. Schneider. 2000. Cloning, chromosome mapping and functional characterization of a human homologue of murine gtse-1 (B99) gene. *Gene.* 254:229–236. http://dx.doi.org/10.1016/S0378-1119(00)00260-2

Monte, M., R. Benetti, G. Buscemi, P. Sandy, G. Del Sal, and C. Schneider. 2003. The cell cycle-regulated protein human GTSE-1 controls DNA damage-induced apoptosis by affecting p53 function. *J. Biol. Chem.* 278:30356–30364. http://dx.doi.org/10.1074/jbc.M302902200

Moore, A., and L. Wordeman. 2004. C-terminus of mitotic centromere-associated kinesin (MCAK) inhibits its lattice-stimulated ATPase activity. *Biochem. J.* 383:227–235. http://dx.doi.org/10.1042/BJ20040736

Nixon, F.M., C. Gutiérrez-Caballero, F.E. Hood, D.G. Booth, I.A. Prior, and S.J. Royle. 2015. The mesh is a network of microtubule connectors that stabilizes individual kinetochore fibers of the mitotic spindle. *eLife.* 4. http://dx.doi.org/10.7554/eLife.07635

Noatynska, A., M. Gotta, and P. Meraldi. 2012. Mitotic spindle (DIS)orientation and DISease: cause or consequence? *J. Cell Biol.* 199:1025–1035. http://dx.doi.org/10.1083/jcb.201209015

Ohi, R., M.L. Coughlin, W.S. Lane, and T.J. Mitchison. 2003. An inner centromere protein that stimulates the microtubule depolymerizing activity of a KinI kinesin. *Dev. Cell.* 5:309–321. http://dx.doi.org/10.1016/S1534-5807(03)00229-6

Orr, B., and D.A. Compton. 2013. A double-edged sword: how oncogenes and tumor suppressor genes can contribute to chromosomal instability. *Front. Oncol.* 3. http://dx.doi.org/10.3389/fonc.2013.00164

Pearson, C.G., and K. Bloom. 2004. Dynamic microtubules lead the way for spindle positioning. *Nat. Rev. Mol. Cell Biol.* 5:481–492. http://dx.doi.org/10.1038/nrm1402

Poser, I., M. Sarov, J.R.A. Hutchins, J.-K. Hériché, Y. Toyoda, A. Pozniakovsky, D. Weigl, A. Nitzsche, B. Hegemann, A.W. Bird, et al. 2008. BAC TransgeneOmics: a high-throughput method for exploration of protein function in mammals. *Nat. Methods.* 5:409–415. http://dx.doi.org/10.1038/nmeth.1199

Ran, F.A., P.D. Hsu, J. Wright, V. Agarwala, D.A. Scott, and F. Zhang. 2013. Genome engineering using the CRISPR-Cas9 system. *Nat. Protoc.* 8:2281–2308. http://dx.doi.org/10.1038/nprot.2013.143

Rankin, K.E., and L. Wordeman. 2010. Long astral microtubules uncouple mitotic spindles from the cytokinetic furrow. *J. Cell Biol.* 190:35–43. http://dx.doi.org/10.1083/jcb.201004017

Rizk, R.S., K.P. Bohannon, L.A. Wetzel, J. Powers, S.L. Shaw, and C.E. Walczak. 2009. MCAK and paclitaxel have differential effects on spindle microtubule organization and dynamics. *Mol. Biol. Cell.* 20:1639–1651. http://dx.doi.org/10.1091/mbc.E08-09-0985

Sanhaji, M., C.T. Friel, N.N. Kreis, A. Krämer, C. Martin, J. Howard, K. Strebhardt, and J. Yuan. 2010. Functional and spatial regulation of mitotic centromere-associated kinesin by cyclin-dependent kinase 1. *Mol. Cell. Biol.* 30:2594–2607. http://dx.doi.org/10.1128/MCB.00098-10

Sanhaji, M., C.T. Friel, L. Wordeman, F. Louwen, and J. Yuan. 2011. Mitotic centromere-associated kinesin (MCAK): a potential cancer drug target. *Oncotarget.* 2:935–947. http://dx.doi.org/10.18632/oncotarget.416

Schvartzman, J.-M., R. Sotillo, and R. Benezra. 2010. Mitotic chromosomal instability and cancer: mouse modelling of the human disease. *Nat. Rev. Cancer.* 10:102–115. http://dx.doi.org/10.1038/nrc2781

Scolz, M., P.O. Widlund, S. Piazza, D.R. Bublik, S. Reber, L.Y. Peche, Y. Ciani, N. Hubner, M. Isokane, M. Monte, et al. 2012. GTSE1 is a microtubule plus-end tracking protein that regulates EB1-dependent cell migration. *PLoS One.* 7:e51259. http://dx.doi.org/10.1371/journal.pone.0051259

Stout, J.R., A.L. Yount, J.A. Powers, C. Leblanc, S.C. Ems-McClung, and C.E. Walczak. 2011. Kif18B interacts with EB1 and controls astral microtubule length during mitosis. *Mol. Biol. Cell.* 22:3070–3080. http://dx.doi.org/10.1091/mbc.E11-04-0363

Talapatra, S.K., B. Harker, and J.P.I. Welburn. 2015. The C-terminal region of the motor protein MCAK controls its structure and activity through a conformational switch. *eLife.* 4. http://dx.doi.org/10.7554/eLife.06421

Tanenbaum, M.E., R.H. Medema, and A. Akhmanova. 2011. Regulation of localization and activity of the microtubule depolymerase MCAK. *BioArchitecture.* 1:80–87. http://dx.doi.org/10.4161/bioa.1.2.15807

Thiru, P., D.M. Kern, K.L. McKinley, J.K. Monda, F. Rago, K.C. Su, T. Tsinman, D. Yarar, G.W. Bell, and I.M. Cheeseman. 2014. Kinetochore genes are coordinately up-regulated in human tumors as part of a FoxM1-related cell division program. *Mol. Biol. Cell.* 25:1983–1994. http://dx.doi.org/10.1091/mbc.E14-03-0837

Thompson, S.L., and D.A. Compton. 2008. Examining the link between chromosomal instability and aneuploidy in human cells. *J. Cell Biol.* 180:665–672. http://dx.doi.org/10.1083/jcb.200712029

Van Stedum, S., and W. King. 2002. Basic FISH techniques and troubleshooting. *Methods Mol. Biol.* 204:51–63.

Walczak, C.E., E.C. Gan, A. Desai, T.J. Mitchison, and S.L. Kline-Smith. 2002. The microtubule-destabilizing kinesin XKCM1 is required for chromosome positioning during spindle assembly. *Curr. Biol.* 12:1885–1889. http://dx.doi.org/10.1016/S0960-9822(02)01227-7

Zhai, Y., P.J. Kronebusch, and G.G. Borisy. 1995. Kinetochore microtubule dynamics and the metaphase-anaphase transition. *J. Cell Biol.* 131:721–734. http://dx.doi.org/10.1083/jcb.131.3.721

Zhang, L., H. Shao, Y. Huang, F. Yan, Y. Chu, H. Hou, M. Zhu, C. Fu, F. Aikhionbare, G. Fang, et al. 2011. PLK1 phosphorylates mitotic centromere-associated kinesin and promotes its depolymerase activity. *J. Biol. Chem.* 286:3033–3046. http://dx.doi.org/10.1074/jbc.M110.165340

Zhang, X., W. Lan, S.C. Ems-McClung, P.T. Stukenberg, and C.E. Walczak. 2007. Aurora B phosphorylates multiple sites on mitotic centromere-associated kinesin to spatially and temporally regulate its function. *Mol. Biol. Cell.* 18:3264–3276. http://dx.doi.org/10.1091/mbc.E07-01-0086

Zhang, Y., F. Buchholz, J.P. Muyrers, and A.F. Stewart. 1998. A new logic for DNA engineering using recombination in Escherichia coli. *Nat. Genet.* 20:123–128. http://dx.doi.org/10.1038/2417

Zong, H., S.K. Carnes, C. Moe, C.E. Walczak, and S.C. Ems-McClung. 2016. The far C-terminus of MCAK regulates its conformation and spindle pole focusing. *Mol. Biol. Cell.* 27:1451–1464. http://dx.doi.org/10.1091/mbc.E15-10-0699